Journal of Energy Storage 113 (2025) 115677

Contents lists available at ScienceDirect

Journal of Energy Storage

journal homepage: www.elsevier.com/locate/est

Review Article

Advances in organic electroactive species for enhancing the performance of all-aqueous redox flow batteries in electrochemical energy storage

Francesco Pileri, Williane da Silva Freitas *, Alessandra D'Epifanio, Barbara Mecheri *

Department of Chemical Science and Technologies, University of Rome Tor Vergata, Via della Ricerca Scientifica, 00133 Rome, Italy

ARTICLE INFO

Keywords:
Renewable energy sources
Electrochemical energy storage
Aqueous organic redox flow batteries
Organic electrolytes
Redox-active molecules
Molecular engineering for enhanced stability and solubility
Voltage window optimization
Enhanced battery performance

ABSTRACT

Aqueous organic redox flow batteries (AORFBs) are emerging as promising energy storage systems due to their scalability, safety, and environmentally friendly nature. This review provides a comprehensive analysis of the recent advances in organic electroactive species for AORFBs, highlighting critical strategies for improving battery performance. After an introduction that outlines the relevance of AORFBs in modern energy challenges, the paper deepens into the working principles and essential components of these systems. Recent developments in organic anolytes and catholytes are discussed, focusing on innovations that enhance redox reversibility, optimize redox potential, and increase solubility and stability under aqueous conditions. A comparative analysis is provided, evaluating these organic species regarding energy density, power density, and cycling stability, demonstrating the improved performance achieved in AORFB systems. The review concludes by identifying future research directions for designing and engineering next-generation organic electrolytes, emphasizing maximizing electrochemical stability and energy storage efficiency to advance the practicality and competitiveness of AORFBs.

1. Introduction

Redox flow batteries (RFBs) have emerged as a decisive technology for grid-scale energy storage, addressing the increasing demand for reliable, high-performance energy management. Their unique design, which separates energy storage from power generation, allows scalability and flexibility crucial in integrating renewable energy sources, such as solar and wind [1–3]. RFBs use redox-active species dissolved in electrolytic solutions pumped through electrochemical cells undergoing charge and discharge cycles. This design decouples the energy capacity from the power output, allowing for increased storage capacity as the volume of the electrolytes in the external tanks increases [2,4]. Storage capacities range from 1 kW to 500 MW, making RFB suitable for residential and industrial applications [4,5].

Developed since the 1980s, Vanadium redox flow batteries (VRFBs) are the most consolidated technology among flow batteries [6], but they still face several limitations that hinder their implementation [7]. One significant concern is the toxicity and environmental impact of vanadium and its compounds. Sustainability issues also arise from the limited availability of vanadium, potentially leading to supply chain vulnerabilities [8]. The corrosive nature of the vanadium electrolytes is another critical limitation. The acidic environment required for optimal performance can lead to the degradation of materials used in the battery components [9–11], leading to increased maintenance costs and a decreased lifetime [12].

Aqueous organic redox flow batteries (AORFBs) that use aqueous-based organic electrolytes offer solutions to the drawbacks of VRFBs, including enhanced safety, reduced maintenance needs, and the potential for environmentally friendly operation [13–18].

Pioneering works investigating the electrochemistry of organic redox compounds as active electrolytes highlighted that quinones, TEMPO (2,2,6,6-tetramethylpiperidin-1-oxyl), and viologens exhibit favorable electrochemical properties for achieving high energy density and efficiency. As demonstrated by Huskinson et al. [19], quinones (particularly derivatives such as 9,10-anthraquinone-2,7-disulphonic acid) are characterized by high water solubility and undergo rapid electron transfer reactions crucial for increasing the energy density of battery systems. Incorporating TEMPO in AORFBs leverages its unique structure, which maintains stability during the redox processes and has enhanced the overall performance of the battery systems [2]. Viologens have also emerged as promising candidates for use as anolytes in aqueous redox flow batteries. Viologens can undergo two-electron transfer reactions,

* Corresponding authors.
E-mail addresses: williane.freitas@uniroma2.it (W. da Silva Freitas), barbara.mecheri@uniroma2.it (B. Mecheri).

https://doi.org/10.1016/j.est.2025.115677
Received 11 December 2024; Received in revised form 23 January 2025; Accepted 1 February 2025
Available online 5 February 2025

making them suitable for high-capacity energy storage applications, but their second redox process is often only partially reversible, and the product formed suffers from low solubility and stability. Advancements in research may address these challenges, enabling the full exploitation of the redox capabilities of this class of molecules. Their water-soluble derivatives have been utilized in neutral AORFBs, demonstrating high performance and stability [20], particularly when paired with other organic compounds like TEMPO [21].

The electrochemistry of quinones, TEMPO, and viologens in RFBs is influenced by factors such as pH, concentration of active species, and electrode materials. Research indicates that quinones' solubility and redox potential can be tuned through chemical modifications, enhancing their performance in alkaline solutions [22]. Similarly, the redox potential of TEMPO and viologens can be adjusted by functionalization with suitable substituents [20], enabling the design of systems with tailored redox potentials and solubilities in water [23,24] that can operate efficiently under varying conditions, including functioning effectively at neutral pH [25]. Operating at a pH close to neutrality minimizes the risk of corrosion and degradation of battery components, a common issue in acidic or alkaline systems [26].

As research advances in this field, AORFBs are likely to play a pivotal role in the future of energy storage, but there are still several challenges to overcome. The primary critical issue is the low solubility of these organic active materials, which affects the energy density and performance of the battery. Additionally, the electrochemical and chemical stability of these compounds is generally lower compared to the inorganic counterparts, leading to capacity fade and shorter battery lifespans. A second aspect that influences the same battery parameters is the crossover of the active species; in many systems, the organic compounds can permeate through the membrane, leading to cross-contamination observing reduced efficiency and capacity retention. Addressing these challenges involves a careful balance of molecular engineering to enhance solubility, stability, and membrane compatibility of the new organic materials, limiting strategies that involve complex, multi-step synthetic processes, which limit scalability and drive-up costs.

Despite the cost of organic materials being technically lower, AORFBs are more expensive than VRFBs due to their low energy density and limited stability, which limits the lifetime of these devices and increases their cost. However, improvements in electroactive species and cell design could make AORFBs a more competitive solution for large-scale energy storage, as highlighted in reviews published in the literature [27–29]. These reviews provide a comprehensive techno-economic analysis of AORFBs, evaluating their cost metrics and associated uncertainties. Through a detailed comparison of capital costs, these studies assess the feasibility of AORFBs in meeting ambitious long-term cost targets for energy storage applications. The potential for cost reduction is also explored, with significant savings anticipated from the mass production of organic active materials. The primary benefits include decreased electrolyte and power costs, although challenges such as plant maintenance remain critical considerations for the widespread adoption of these systems.

2. Overview of AORFB: working principle and components

RFBs are classified into aqueous and non-aqueous systems, each presenting unique advantages and challenges. Aqueous RFBs, such as vanadium and iron-chromium systems, benefit from high ionic conductivity and safety due to their water-based electrolytes, making them suitable for large-scale applications [30]. Conversely, non-aqueous RFBs utilize organic solvents, which can enhance energy density and operational voltage, but often face issues related to solvent stability and environmental impact [31,32].

Among these technologies, AORFBs emerge as a promising solution. They combine the safety and efficiency of aqueous systems with the high energy density of organic compounds, offering a sustainable alternative for energy storage, demonstrating significant potential for grid-scale applications, effectively addressing the intermittency of renewable energy sources while minimizing environmental concerns associated with traditional non-aqueous systems.

AORFBs operate by utilizing redox-active organic molecules dissolved in an aqueous electrolyte, which circulate between two electrodes. The primary components include electrodes, typically made of conductive materials, a membrane separator to prevent cross-contamination of the electrolytes, and the electroactive species (organic compounds like quinones or viologens) and storage tanks. The electroactive species, dissolved in aqueous solutions, are stored in two different tanks (anolyte and catholyte) and separately pumped to the electrode surface where the redox reaction occurs in the respective half-cells. Fig. 1 shows a schematic of an AORFB system.

The redox reactions in AORFBs involve the oxidation of the anolyte at the anode and the reduction of the catholyte at the cathode, allowing for the storage and release of energy. This system enables the decoupling of energy and power, as the volume of the electrolyte determines the energy capacity, while the surface area of the electrodes influences the power output.

The performance of an AORFB can be evaluated using the following parameters:

ENERGY DENSITY: major parameter used to describe battery performance. It describes the average energy stored per unit of volume (Wh L^{-1}). Its theoretical value can be calculated by Eq. (1):

$$E = n\,C\,F\,\Delta U \tag{1}$$

where n is the number of electrons involved in the process, C (M) is the concentration of the redox active material, F is the Faraday constant, ΔU (volts) is the potential difference between the anolyte and catholyte redox processes. It is easy to figure out how the solubility of the electroactive species and their redox potential difference need to be maximized to increase the energy density. In most of the cases, the practical energy density is lower compared to the theoretical one and can be expressed according to Eq. (2):

$$E = \frac{\int i\,V(t)\,dt}{3.6\,V} \tag{2}$$

where i is the current (A), $V(t)$ is the voltage over time, and V is the total volume (L).

2.1. Coulombic efficiency (CE)

It indicates how effectively a battery can store and release charge and can be calculated by discharge and charge capacity ratio, according to Eq. (3):

$$CE = \frac{Discharge\ capacity\ (Ah)}{Charge\ capacity\ (Ah)} \cdot 100 \tag{3}$$

Due to irreversible side reactions and crossover, CE generally decreases over cycling.

2.2. Voltage efficiency (VE)

It measures how effectively a battery utilizes voltage during its charge and discharge cycles and is defined as the ratio of the average discharge voltage to the average charge voltage of the battery over a full charge-discharge cycle. It can be expressed according to Eq. (4):

$$VE = \frac{Average\ discharge\ Voltage\ (V)}{Average\ charge\ Voltage\ (V)} \cdot 100 \tag{4}$$

VE is lower than 100 % because of electrochemical, ohmic, and concentration overpotential.

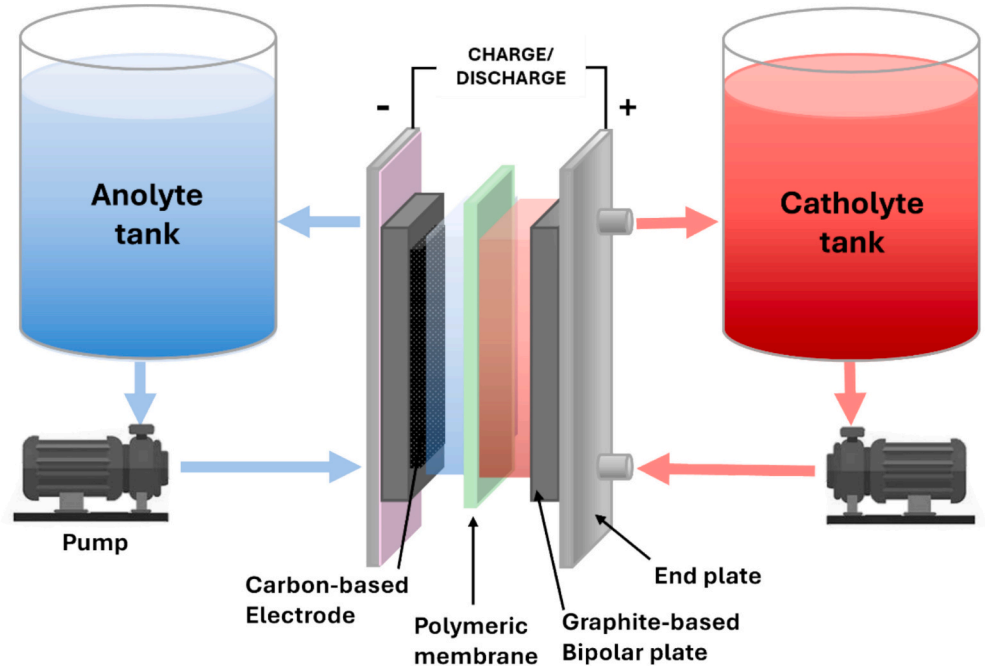

Fig. 1. Schematic of an AORFB system.

2.3. Energy efficiency

It can be expressed as the product of CE and VE and represents the percentage of energy that can be recovered from a battery during discharge compared to the energy supplied during charging (when a constant charging-discharging current is applied).

2.4. Power density

Power density refers to the amount of power (energy delivery rate) the battery can provide per unit of geometric area of the electrodes (W cm^{-2}), per volume of the electroactive solution (W L^{-1}), or mass of the electroactive species (W kg^{-1}). It is usually reported in W cm^{-2} or W L^{-1} units, and the latter is mainly considered to provide information on how much power the system can deliver relative to the size of the electrolyte storage tanks, which helps to identify its suitability for specific applications considering space or weight constraints. The higher the power density, the higher the energy output relative to the volume and concentrations of the electroactive solutions, which benefits the system's scalability.

2.5. Theoretical capacity

The theoretical capacity of a battery represents the ideal amount of charge (often measured in ampere-hour per Liter, Ah L^{-1}) that could be extracted from the battery under perfect conditions without any losses or inefficiencies. It can be calculated using the following equation (Eq. (5)):

$$Theoretical\ Capacity = \frac{n\,F\,C}{3600} \tag{5}$$

where n is the number of electrons involved in the redox process, F is the Faraday constant and C (M) is the concentration of the electroactive species.

2.6. Capacity utilization

Battery capacity utilization refers to how effectively a battery's available energy storage capacity is used. It measures the actual energy output from the battery relative to its theoretical maximum. This measure can be affected by several factors, including charge and discharge rates, operating temperature, depth of discharge, and the overall efficiency of the battery management system.

2.7. Capacity retention

It is an important parameter used to describe the ability of a battery to retain its original capacity over time or after a certain number of charge-discharge cycles. It is an indicator of the battery's stability. Capacity retention is generally expressed as a percentage of the initial capacity of the battery and can be expressed according to Eq. (6):

$$Capacity\ retention_{n^{\circ}cycle} = \frac{Capacity_{n^{\circ}cycle}}{Initial\ Capacity} \cdot 100 \tag{6}$$

It can also be expressed as capacity decay, a percentage of capacity loss per cycle or day.

In AORFBs, the performance is significantly influenced by three critical components: the electrode, membrane separator, and electroactive species.

The role of the separator (usually as a polymer membrane) is to separate the different half-cells, avoiding cross-contamination and enabling ion transport to balance the redox process. For this reason, they have a crucial role in RFBs. The most common class of membranes utilized is ion exchange membranes, specifically cation exchange membranes (CEMs), anion exchange membranes (AEMs), and amphoteric ion exchange membranes (AIEMs), depending on the type of functional charged groups, thus dictating the operational pH of AORFB.

CEMs are typically used in acidic to neutral environments, while AEMs are advantageous in alkaline conditions due to the poor conductivity for hydroxide ions of CEMs and stability issues at high pH values [33–38]. AIEMs have two types of functional groups, providing cationic and anionic features in one single membrane. Cationic groups' presence helps prevent the crossover of larger cationic metal species. In contrast, the presence of anionic groups generally enhances the ionic conductivity of small cations (*i.e.*, H^+ and K^+), combining the advantages of CEMs and AEMs in a single membrane [39].

Nafion membranes are the most representative commercial CEMs

[40], widely used in vanadium-based inorganic RFBs [41–43] and extensively explored in AORFB [19,25,44,45]. Other commercial CEMs and AEMs used in AORFBs include Fumasep E-620 K [46], Fumasep FAA-3-PE-30 [47], Selemion CSO [48] and Selemion DSV [49] membranes.

Polyaromatic membranes have emerged as a promising candidate for tailoring the size of the ion transport channels by microphase separation, thus minimizing crossover effects [50]. Sulfonated polyether ether ketone (SPEEK) membranes have demonstrated good mechanical strength and thermal stability, essential for demanding conditions in AORFBs and high ionic conductivity [51]. Their tunable properties through sulfonation can enhance ionic conductivity while maintaining structural integrity [52]. Polybenzimidazole (PBI) exhibits excellent thermochemical and mechanical stability at a lower cost than the commercially benchmark materials [53,54]. Although PBI is one of the most promising low-cost non-fluorinated polymers, developing stable PBI-based membranes with fast and selective ion transport channels remains challenging [55,56].

In addition, exploring size-exclusion membranes as alternatives to Nafion in AORFB has recently attracted considerable interest. Size-exclusion membranes function primarily through size sieving, allowing ions or molecules to pass based on their size relative to the membrane porosity. Research has shown that size-exclusion membranes, such as low-cost commercial dialysis membranes, can effectively replace expensive ion-exchange membranes like Nafion, providing a cost-effective solution without compromising performance [57–59]. In addition to size exclusion, the Donnan effect can also enhance the selectivity of membranes. Combining size and charge-based exclusion mechanisms can minimize crossover, which is critical for AORFBs operation [60,61].

The choice of electrode materials is critical in optimizing the performance of AORFBs. Carbon-based materials such as carbon cloth, carbon felt, and carbon paper are widely used as electrodes in AORFB due to their high electrical conductivity, mechanical stability, and compatibility with various electrolytes [62–65]. Functionalization strategies for these carbon materials can significantly improve their electrochemical properties. Studies have shown that incorporating conductive additives or modifying surface chemistry can enhance charge transfer rates and increase the stability of the electrodes during cycling [66–70]. Developing composite materials that combine carbon with other conductive or electrocatalytic materials has also been explored to enhance performance further [71,72].

Although the separator membrane and electrodes play a fundamental role in optimizing the performance of AORFBs, the design of organic redox electroactive species is the most influential factor in advancing AORFB technology, as these species directly impact the energy density, cycling stability, and overall efficiency of the system.

Another critical factor affecting the RFB performance is temperature. Given the practical applications of these devices, their compatibility with environmental conditions, particularly temperature, is crucial. Temperature significantly impacts key parameters such as the conductivity and viscosity of the solution, the capacity and efficiency, the stability and solubility of electrolyte materials, and the stability of the membrane. To ensure the efficiency of these commercially available devices, a thermal management system is essential for maintaining thermal fluctuations within a safe temperature range tailored to the specific characteristics of the device, which results in increased costs and maintenance requirements. However, temperature-stability investigations of AORFBs are scarcely conducted, except a few highly relevant studies that have explored the thermal stability of certain organic electrolytes, particularly from the perspective of their potential use in AORFBs operating in regions of the world characterized by extreme temperature conditions, including both severe heat [73] and intense cold [74,75].

3. Most recent innovations in electroactive organic species for enhanced AORFB performance

3.1. Requirements and challenges of organic electrolytes for AORFB applications

The design of optimal organic electrolytes necessitates considering several critical properties, including solubility, redox potential, stability, and reaction kinetics [76].

One of the primary requirements for organic electrolytes in AORFBs is high solubility in an aqueous environment to ensure sufficient concentrations of redox-active species. Designing and using highly soluble molecules is a common strategy, and the functionalization of poorly soluble organic molecules with polar moieties is a common strategy to enhance solubility [77,78].

Another critical requirement is optimizing the redox potential of the organic molecules used. The redox potential directly influences the battery's energy density and voltage output [79]. Molecular engineering approaches are often employed to tailor the redox properties of organic compounds, allowing for the design of materials that can operate at higher voltages and deliver better performance [80,81]. However, this must be balanced with the need for stability and reversibility. Indeed, redox couples must undergo highly reversible oxidation and reduction reactions with minimal side reactions. Redox reactions must occur with fast kinetics and low overpotential to ensure that the redox-active species can undergo rapid oxidation and reduction at the electrodes. This minimizes power loss and improves the overall efficiency of the battery.

Additionally, the redox couple's oxidized and reduced forms must exhibit high electrochemical stability over many charge/discharge cycles. Instability can lead to degradation of redox-active species, resulting in loss of capacity and shortened battery life. Research has shown that the structural design of these molecules can significantly impact their stability; modifying the molecular structure can enhance resistance to degradation [82,83] and the choice of supporting electrolytes and solvents can influence the solvation dynamics and stability of the redox-active species [44,79,82,84–87].

Furthermore, the interaction between the electrolyte and the membrane is crucial, as it must allow for selective ion transport while preventing the crossover of redox-active species, which can lead to self-discharge and reduced efficiency.

3.2. Overview of the main classes of molecules used as organic electrolytes in AORFBs

Quinones are one of the most widely studied classes of organic molecules for AORFBs. Anthraquinones, benzoquinones, and naphthoquinones derivatives have been extensively studied because their redox potentials can be fine-tuned by chemical modification [88–97]. Despite their promising properties, quinones are prone to degradation through side reactions such as nucleophilic attack by water, leading to capacity fading over time.

Viologens are widely investigated as anolytes in AORFBs due to their high solubility in water and stable redox properties. Modifying their molecular structure can easily adjust their redox potential, making them versatile for various battery configurations [98–102]. However, viologens can suffer from dimerization, dealkylation, and other side reactions, which limit their long-term cycling stability [103–105]. Reducing crossover through the membrane is also a significant challenge [47,105,106].

Nitroxide radicals, such as 2,2,6,6-tetramethylpiperidine-1-oxyl (TEMPO), are commonly used as catholytes in AORFBs due to their fast redox kinetics, stability, and excellent solubility in water, leading to high power density in flow battery systems [107,108]. TEMPO and its derivatives can degrade *via* side reactions such as ring-opening or polymerization, particularly in the presence of nucleophilic attack by water molecules.

Ferrocene is known for its well-defined and reversible redox chemistry, making it highly suitable for energy storage applications [18,44,73]. Although it undergoes single electron oxidation with fast redox kinetics and has a highly stable redox behavior, its solubility in aqueous electrolytes tends to be lower than other organic molecules such as quinones or viologen.

Aromatic heterocyclic compounds such as phenothiazines, pyrazines, phenoxazine, pyridoxal, carbazoles, phenazines, naphthalene, bipyridine, fluorenones, verdazyles, and alloxazines have also been investigated as redox-active materials for AORFBs [78,109–117]. These molecules often have good stability and can undergo multi-electron transfer reactions, making them attractive for high-energy-density applications. These compounds offer a wide range of tunable properties. Depending on their functionalization, they can be used for both anolyte and catholyte applications. Still, like other organic molecules, aromatic heterocycles can undergo degradation during long-term cycling, requiring careful molecular design to improve their robustness and solubility.

In this article, we will focus our attention on the most recent innovations published in the literature regarding the design, molecular engineering, and optimization of new TEMPOs and metal-organic complexes as catholytes and quinones, viologens and aromatic heterocyclic compounds as anolytes for AORFB applications (Fig. 2).

3.2.1. *Recent advances in organic catholytes for AORFBs*

Among the potential candidates, 2,2,6,6-tetramethylpiperidine-1-oxyl (TEMPO), a nitroxide radical, is a promising molecule for improving the capacity and efficiency of AORFBs.

TEMPO has excellent chemical and electrochemical properties, such as low molecular weight, high redox potential (0.57 V *vs* SHE), fast redox kinetics, and good chemical and electrochemical stability). However, its low solubility in aqueous electrolytes (approximately 0.07 M) hinders the practical application of TEMPO in AORFBs. Recent breakthroughs, such as improving the solubility of TEMPO by using lithium bis(trifluoromethanesulfonyl)imide (LiTFSI), have opened up new possibilities for the practical use of non-functionalised TEMPO as a catholyte in AORFBs. Pedraza et al. proposed a strategy to increase the water solubility of TEMPO using LiTFSI as a supporting salt [118]. With this approach, the solubility of TEMPO, starting from a value of 4.4 M in 1 M LiTFSI, reached 5.6 M in 5.0 M LiTFSI, which is 80 times higher than its solubility in water alone. Although this increase in solubility allows for higher energy densities in flow batteries, which can significantly improve their performance in large-scale energy storage applications. It is important to note that excessively high electrolyte concentrations can increase the solution viscosity, thereby reducing ionic conductivity to levels that may render it impractical for battery applications. Viscosity studies conducted by the authors on a 10 mM TEMPO solution in 4 M LiTFSI resulted in a dynamic viscosity of 11 mPa s. It would be valuable to perform similar studies using electrolyte concentrations that are more representative of those used in battery testing. The enhanced solubility of TEMPO in aqueous LiTFSI solutions results from a unique interaction between the TEMPO molecules and the TFSI anion, reducing the number of interactions between TEMPO molecules and promoting their dissolution in the supporting electrolyte. This approach does not require any chemical modification of TEMPO, preserving its electrochemical properties while improving its solubility in aqueous systems.

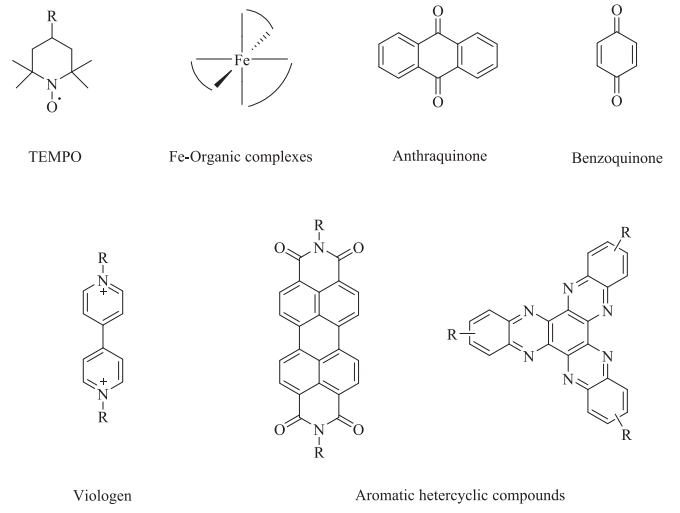

Fig. 2. Scheme of the classes of molecules discussed in this article.

The electrochemical performance of highly concentrated TEMPO catholytes (0.1 to 1 M in 4 M LiTFSI) was tested in symmetric AORFBs, demonstrating excellent performance. Using 1 M TEMPO solution led to a volumetric capacity of 23.85 Ah L^{-1} at 2.5 mA cm^{-2}, corresponding to 89 % theoretical capacity utilization, 98.3 % coulombic efficiency, and long-term cycling stability with a capacity fade of 0.082 % per day. The good AORFB performance arising from the reversibility and fast kinetics of the redox reactions in TEMPO-based, as confirmed by cyclic voltammetry studies, showing a diffusion coefficient of 8.9×10^{-7} cm^2 s^{-1} and a kinetic rate constant k^0 of 0.018 cm s^{-1}, both favorable for efficient charge-discharge cycles in RFB systems. Finally, a neutral pH AORFB with 0.5 M TEMPO in 4.0 M LiTFSI and 0.25 M $(SPr)_2V$ in 4.0 M LiTFSI with a theoretical OCV of 1.08 V was assembled. The capacity achieved was 9.47 Ah L^{-1} at 7.5 mA cm^{-2} (70.7 % of theoretical), decreased to 9.0 Ah L^{-1} at 20 mA cm^{-2}, and a long-term-stability test was also carried out cycling at 10 mA cm^{-2} over 285 cycles. This evidence showed a capacity utilization of 69 % and a capacity decay rate of 0.048 %/cycle or 0.60 %/day with a total capacity retention of 86.4 % (average CE of 99.5 % and EE of 82 %).

Along with solubility, redox potential, diffusion coefficient, and electron transfer rate constant can be improved by modifying TEMPO with appropriate functional groups. Fig. 3 shows the chemical structure of different TEMPO derivatives.

Despite recent advantages, the crossover of neutral or single-charged TEMPO derivates remains challenging. To overcome this limit, Pan et al. proposed a highly soluble crossover-free N-heterocycle-substituted TEMPO [108]. By designing highly water-soluble materials with

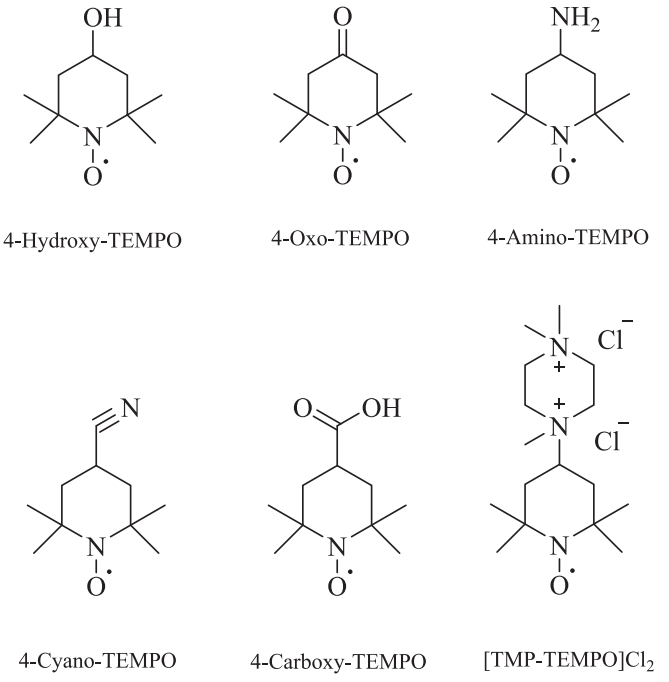

Fig. 3. Chemical structure of six TEMPO derivatives. Adapted with permission from Ref. [119] with permission from the Royal Society of Chemistry.

multiple positive charges, the redox pair generates a strong Gibbs-Donnan effect that prevents the active molecules from permeating through the membrane, thus avoiding cross-contamination between the anolyte and catholyte compartments. Starting with oxo-TEMPO, two synthesis steps are required to obtain the desired product (TMP-TEMPO), an initial coupling *via* Borch reduction followed by *N*-methylation to create two positive charges on the molecule. The N-heterocycle substitution introduces positive charges, which increase the water solubility of TEMPO to 2.4 M in deionized water, 2.25 M, and 2.16 M in 1.0 M and 2.0 M NaCl solution, respectively. Cyclic and linear sweep voltammetry was performed in 0.5 M NaCl to investigate the electrochemical properties. CV shows that TMP-TEMPO follows a diffusion-controlled redox process at 0.98 V (*vs* SHE) with reversible behavior. LSV analysis gave a diffusion coefficient of around 3.85×10^{-6} $cm^2\ s^{-1}$, and the kinetic rate constant obtained was also favorable, with a registered value of k^0 of 1.65×10^{-2} cm s^{-1} and observing no crossover through the AMVN anion exchange membrane.

In addition to TEMPO-based catholytes, which have gained popularity as efficient, metal-free redox-active materials, metal-containing organic molecules are also employed as catholytes in AORFBs. These metal-containing compounds, often based on coordination complexes or organometallic frameworks, offer several advantages. Metal centers can enhance redox potential, provide additional stability to the redox-active sites, and broaden the electrochemical window. This can lead to improved energy density and enhanced cyclability, making them attractive candidates for AORFB applications. Iron is the most abundant and inexpensive transition metal in nature. Among the Fe complexes, the organic ones possess all the critical properties required for AORFB applications, such as the ability to exploit the metal redox process, the tunability of its potential and solubility through the adoption of different organic ligands, and low crossover permeability due to its large molecular size. To achieve high energy density, high voltage, and high electrolyte solubility, Li et al. proposed a rational design of an Iron^{II} complex catholyte involving a functionalized 2,2′-Bipyridine (Bpy) ligand [120]. Bpy is a well-known non-aqueous ligand that increases the electrochemical potential of its Fe complex. In this work, two different approaches have been used to achieve its high water solubility: ligand functionalization with hydrophilic functional groups and a change in molecular symmetry. The first strategy was adopted through a carboxylic acid Bpy functionalization (Dcbpy), which, due to its electron-withdrawing property, additionally increases the Iron oxidation potential to synthesize $Na_4[Fe^{II}(Dcbpy)_3]$.

The second strategy was to break the complex symmetry by adding a second ligand (cyanide) to form $Na_4[Fe^{II}(Dcbpy)_2(CN)_2]$ and $Na_4[Fe^{II}(Dcbpy)(CN)_4]$ (Fig. 4). In addition, using two different ligands allows precise tuning of the complex's properties, theoretically enabling the desired properties to be obtained. The solubility of all the synthesized materials was measured by UV–Vis spectroscopy analysis. The values obtained in pure water are shown: 0.26 M, 1.09 M, and 1.02 M for $Na_4[Fe^{II}(Dcbpy)_3]$, $Na_4[Fe^{II}(Dcbpy)_2(CN)_2]$ and $Na_4[Fe^{II}(Dcbpy)(CN)_4]$, respectively. The characterization continued with CV measurements in a 0.5 M NaCl solution to obtain a redox potential value of 0.26 V, 0.41 V, 0.65 V and 0.9 V (*vs* Ag/AgCl) for $Na_4[Fe^{II}(CN)_6]$, $Na_4[Fe^{II}(Dcbpy)(CN)_4]$, $Na_4[Fe^{II}(Dcbpy)_2(CN)_2]$ and $Na_4[Fe^{II}(Dcbpy)_3]$, respectively. In addition, the diffusion coefficients were measured by LSV analysis, exhibiting a value of 2.3×10^{-6} $cm^2\ s^{-1}$ for $Na_4[Fe^{II}(Dcbpy)_2(CN)_2]$.

Initial flow battery tests were performed using $Na_4[Fe^{II}(Dcbpy)_2(CN)_2]$ as catholyte and 1,1′-bis(3-sulfonatopropyl)-4,4′-bipyridinium (SPr-Bpy) as anolyte at a concentration of 0.1 M and a pH of 7.0. With a cell voltage of 1.2 V, the device exhibited a capacity of 84.2 % to 66.7 % of the theoretical one at current densities from 20 to 100 mA cm^{-2}, respectively. To assess catholyte stability, a second battery test was carried out with an anolyte: catholyte ratio of 2.1:1, in a cut-off voltage range of 0.8-1.35 V. The capacity utilization of the catholyte reached 85 %, and after 6000 cycles, the total capacity retention was 90.5 %, corresponding to a decay ratio of 0.00158 % per cycle. The energy and voltage efficiencies through the cycles remained at around 73.80 ± 0.04 %, with an average coulombic efficiency of 99.75 ± 0.04 %. When the cut-off voltage was set to 1.4 V, the catholyte capacity utilization increased to 90.5 %, but during the subsequent 2500 cycles, a capacity decay of 0.00283 % per cycle was observed, even though NMR analysis showed no catholyte degradation. Further tests using $Na_4[Fe^{II}(Dcbpy)(CN)_4]$ as the catholyte showed 81.6 % to 73.8 % capacity utilization at 40 to 100 mA cm^{-2} current density, and the cell also showed good cyclability, with a capacity degradation rate of 0.03 % per cycle over the first 1000 cycles. Finally, high energy density, capacity balanced AORB was assembled near the limit concentration 1.02 M of $Na_4[Fe^{II}(Dcbpy)_2(CN)_2]$. Under this condition, with a theoretical capacity of 27.4 Ah L^{-1}, the energy density reached the value of 17.5 Wh L^{-1}; at a current density of 24 mA cm^{-2}, the cell showed a capacity utilization of 73 % and a practical energy density of 12.5 Wh L^{-1}. In the first 250 cycles, a capacity decay rate of 0.1 % per cycle was observed, mainly attributed to anolyte crossover and degradation.

A further step could be to harness all the properties and benefits described above through a biomimetic approach. Yang et al. proposed a bio-inspired multi-coordination sphere containing cyclodextrin, naphthol green B (NGB), and Fe as catholyte for AORFB application [121]. NGB is a commercially available dye consisting of 1-nitroso-2-naphthol-6-sulphonic acid sodium Iron salt. It is attractive due to its low cost and excellent redox properties, particularly its Fe(III)/Fe(IV) redox couple. NGB has demonstrated a redox potential of 0.73 V *vs.* NHE under neutral conditions, providing an alternative to the more expensive and less stable materials typically used in redox flow batteries. Unfortunately, the CV registered presented a weaker reduction peak compared to the oxidation one; however, when hydroxypropyl β-cyclodextrin (HP-β-CD) and γ-CD were solubilized (second coordination sphere) in the electrolyte solution, reversible redox peaks were registered at 0.71 V and 0.77 V, respectively. This positive effect was not registered when α-CD was added, and the CV curves remained almost identical. The main difference between these 3 CDs is the diameter of the inner hydrophobic

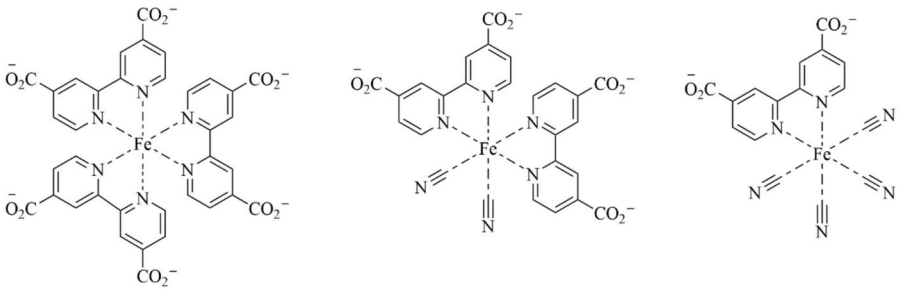

Fig. 4. Structure of the three different Fe complexes.

region. The hydrophobic cavity dimension of HP-β-CD is compatible with that of the NGB. For this reason, a bound stable inclusion complex is formed, creating a first coordination sphere formed by ligands, the CD cavity as a secondary coordination sphere, and the peripheral functional groups of CD as a third coordination sphere (Fig. 5). The NGB enclosed in the HP-β-CD undergoes a redox reaction without dissociating from the inclusion; the active site on the electrode surface is electrochemically oxidized, and the oxidized NGB can continue to bind to the HP-β-CD, thus improving the stability of the molecule.

In contrast, α-CD and γ-CD have a too-small or too-large cavity volume, as indicated by ^{1}H NMR analysis showing an upfield chemical shift of the naphthalene protons pointing to its insertion into the HP-β-CD cavity. EIS measurements showed improved electrochemical kinetics when HP-β-CD was added to the solution. Only a slight increase of the solution viscosity was recorded, reaching a value of 1.14 mPa s at an HP-β-CD concentration of 0.02 M. Despite an NGB solubility of 34 mM, adding 0.1 M and 0.3 M HP-β-CD allows an NGB solubility increase to 0.21 M and 0.25 M, respectively.

The electrochemical properties were investigated by CV analysis of 4 mM NGB with 8 mM HP-β-CD, revealing a reversible, diffusion-controlled redox process. In addition, the diffusion coefficient and transfer rate constant of NGB were also evaluated by LSV and showed a value of $D = 2.80 \times 10^{-7}$ cm^2 s^{-1}, $k^0 = 1.52 \times 10^{-3}$ cm s^{-1}. A full battery test was performed using 0.01 M NGB, 0.02 M HP-β-CD in 1.0 M NaCl solution as the catholyte, and 0.01 M $(Spr)_2V$ in 1.0 M NaCl solution as the anolyte, achieving a high battery voltage of 1.22 V. A 1.33 to 0.32 mAh capacity was recorded at current density range of 5.0 to 30 mA cm^{-2}.

Similarly, the EE and VE decreased with increasing current density from 54 % at 5 mA cm^{-2} to 23 % at 30 mA cm^{-2}, while the CE remained above 99 % for all tests. To extend the study to long cycling stability, 800 cycles were performed at a current density of 10 mA cm^{-2} under the same conditions. The battery retained 99 % of its initial capacity, corresponding to a capacity fade rate of 0.0125 % per cycle. The CE was also close to 100 %, and a peak power density of 19.4 mW cm^{-2} was recorded. Post-mortem analysis showed that the low capacity fade was due to the crossover of anolyte across the Nafion 212 membrane. A higher concentration battery was assembled: 0.1 M NGB with 0.2 M HP-β-CD in 1.0 M NaCl solution as catholyte and 0.1 M $(Spr)_2V$ in 1.0 M NaCl solution as anolyte. In the current density range of 5 to 35 mA cm^{-2}, the device showed a capacity of ~9.4 mAh to ~6.0 mAh and a maximum EE of 80 % at 5 mA cm^{-2}. After 250 cycles at 10 mA cm^{-2}, the capacity remained at 98 % with a capacity decay of 0.008 % per cycle. Unfortunately, the 0.2 M NGB/$(Spr)_2V$ battery exhibited a low CE, probably due to the high viscosity and low conductivity of the high concentration of the electrolyte solution.

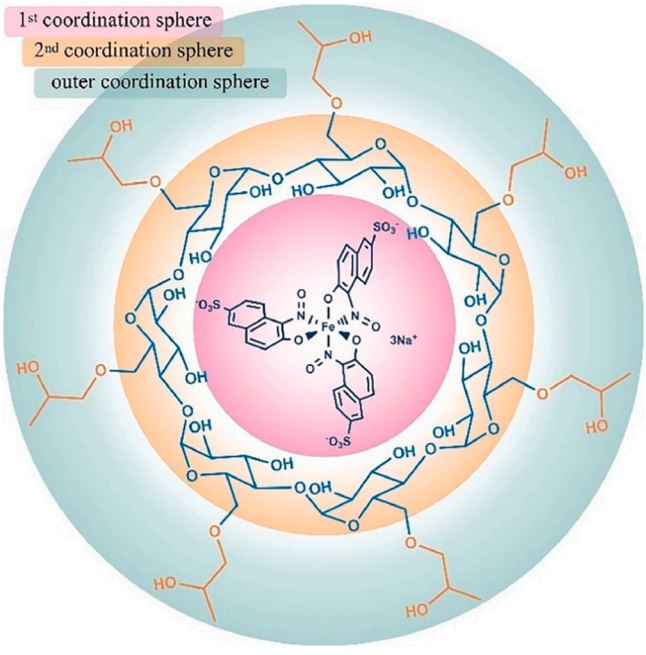

Fig. 5. Representation of NGB 1st, 2nd, and outer coordination sphere. Reproduced from Ref. [121] with permission from Elsevier.

3.2.2. *Recent advances in organic anolytes for AORFB*

In recent years, quinones have gained attention as suitable candidates for AORFBs due to their redox stability, tunability, and potential to replace metal-based systems. Most quinone-based batteries, however, have operated in acidic or alkaline conditions, which introduces side reactions and limits cycle life [93]. The study published by Yang et al. is based on developing a neutral aqueous all-quinone redox flow battery to overcome these limitations while optimizing performance and stability [88]. In this work, five quinones differing in the number and position of the sulfonate groups were studied in neutral aqueous conditions (Fig. 6); neutral conditions significantly reduce the corrosiveness of the electrolyte, minimizing material degradation and prolonging the life of cell components such as membranes and electrodes, in addition, side reactions common in acidic and alkaline systems, such as hydrogen evolution and degradation of quinones, are minimized in neutral conditions, resulting in improved long-term cycling stability. All species showed good electrochemical reversibility, but only 2,7-AQDS (displaying a redox process around -0.3 V *vs NHE*) showed a high solubility of 1.39 M in water compared to the other four quinones (less than 70 mM), demonstrating that even minor differences in functionalization can have a significant impact on the hydration sphere. The supporting salt also affects the solubility of the solute. Therefore, several organic and inorganic salts have been tested with 2,7-AQDS. It was found that the lower the salt's capacity to establish hydrogen bond interaction with water, the greater the quinone solubility; for this reason, Na_2SO_4 was chosen as the best-supporting electrolyte among those studied. To optimize the salt concentration in terms of the viscosity of the solution, tests were carried out with different concentrations, obtaining a dynamic viscosity value ranging from 1.12 mPa s in a 0.25 M Na_2SO_4 solution to 1.45 mPa s in a 0.75 M Na_2SO_4 solution. Although the high solubility of 1.39 M 2,7-AQDS was achieved, its reduced form has a solubility of 0.25 M in 0.5 M Na_2SO_4 solution. Hence, a 0.2 M 2,7-AQDS in 0.5 M Na_2SO_4 solution coupled with 0.2 M HQS in 0.5 M Na_2SO_4 was used for a cell test. At current densities from 40 to 60 mA cm^{-2}, the device showed a capacity utilization from 71.0 % to 70.1 % and an energy efficiency from 73.5 % to 64.88 %, respectively. Furthermore, a power density of 54.1 mW cm^{-2} was recorded at 100 % state of charge (SOC). The long-term cycling test was performed at a current density of 60 mA cm^{-2}, displaying a cell voltage 0.9 V. Columbic efficiency remained constant at over 96 % for all 120 cycles with capacity utilization of 7.5 Ah L^{-1}, and EE and VE remained above 56 % and 61 %, respectively.

Benzoquinones (BQs) are considered among the most promising candidates due to their fast and reversible redox properties, high specific capacity, and environmental compatibility. The introduction of hydroxyl (-OH) groups to benzoquinones has emerged as a potential strategy to improve the stability and performance of these materials, and the study by Kim et al. investigates the effect of hydroxyl functionalization on the electrochemical behavior, cycling stability, and overall performance of BQ derivatives in alkaline RFB systems [122]. The study focuses on a series of hydroxylated BQ derivatives, including 2-hydroxybenzoquinone (HBQ), 2,5-dihydroxybenzoquinone (DHBQ), and tetrahydroxybenzoquinone (THBQ) (Fig. 7), comparing their performance with bare p-benzoquinone (BQ). The aim is to assess how the number and position of the hydroxyl groups affect the electrochemical stability and capacity retention of these molecules during extended cycling. Electron-donor hydroxyl groups increased the electron density on the BQ core, resulting in a negative shift in the redox potential and

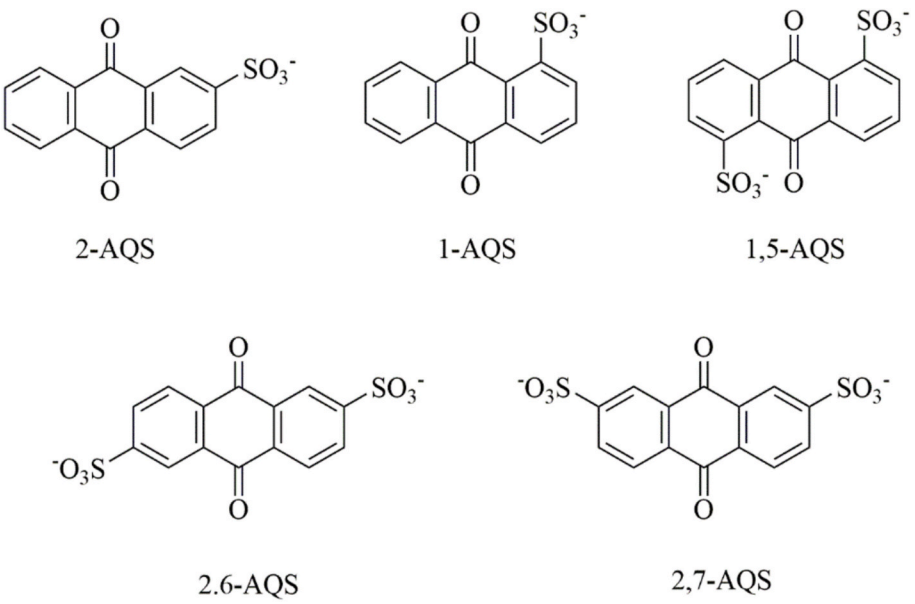

Fig. 6. Five different quinone derivatives structure.

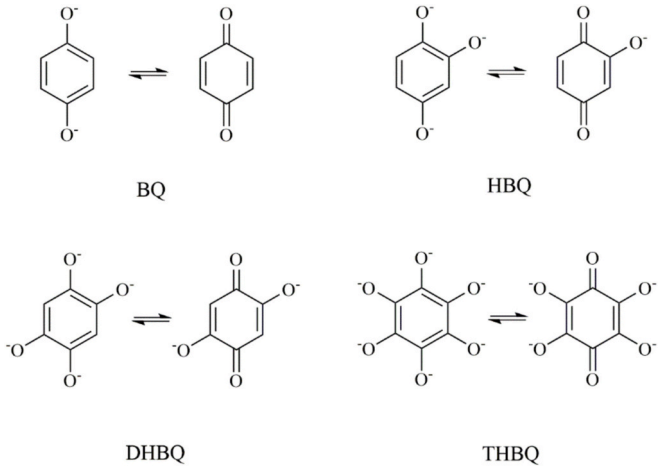

Fig. 7. Redox processes of four BQ derivatives. Reproduced from Ref. [122] with permission from Elsevier.

enhancing the resistance of BQs to nucleophilic attacks, a common cause of degradation in alkaline environments.

Moreover, hydroxyl groups promote solubility in aqueous solutions, particularly in alkaline conditions, further contributing to better battery performance. Cyclic voltammetry was used to investigate the electrochemical behavior of the synthesized hydroxylated benzoquinone, indicating how -OH groups in the para position of the redox active center ketone groups electrochemically stabilize the molecule and how excessive functionalization can induce excessive repulsive force and open up different degradation pathways. Another fact worth mentioning is the active form of the BQs present in the 1 M KOH: while BQ, HBQ, and THBQ were mainly observed in the reduced (enolate) form, DHQB retained the oxidized (quinone) form, because of which two different catholyte conditions were required for the battery tests.

The DHQB-based battery was assembled with an anolyte concentration of 0.5 M in a 1.0 M KOH solution and 0.4 M ferrocyanide ($K_4Fe(CN)_6$) in 1.0 M KOH as the catholyte. The first charge at a current density of 32 mA cm^{-2} and a voltage cut-off of 0.6 V and 1.7 V showed a capacity close to 100 %, reaching 85.7 % by the 10th cycle and about 60 % by the 50th. To investigate the cause of the capacity fade, post-mortem NMR analyses were carried out, and some minor peaks appeared in contrast to the pre-cycling spectra; these peaks were attributed to different degradation pathways leading to the formation of malonate and acetate ions.

Viologens are also recognized for their promising performance as anolytes in AORFBs thanks to their favorable redox potentials and stability. However, optimizing viologens for AORFBs requires the consideration of several interrelated factors, including solubility, viscosity, stability, membrane permeability, and electrochemical performance [14,123–126]. Sullivan et al. investigated different combinations of viologen functionalization based on a single-step hydrothermal method [127]. Traditional methods of viologen synthesis rely on multi-step reactions in organic solvents, which often result in low yields and require purification steps. The new hydrothermal approach eliminates these inefficiencies by enabling a high-yield reaction using low-cost chlorine-terminated functionalization units (Fig. 8). The electrochemical performance of the synthesized viologen derivatives was characterized by cyclic voltammetry (CV) and electrochemical impedance spectroscopy (EIS). All viologens displayed reversible redox behavior with fast electron transfer kinetics, as indicated by their standard rate constants (k^0) greater than 10^{-2} cm s^{-1}. This suggests that the Faradaic resistance in the system is minimal, supporting the efficient cycling of the battery. The viologens' formal redox potentials (E^0) ranged from −0.320 to −0.383 V *vs* SHE, demonstrating viologens' chemical stability under cycling conditions, particularly their resistance to degradation in neutral and alkaline pH environments. Viologens with secondary alcohol groups showed improved resistance to nucleophilic attack by hydroxide ions, which is critical for maintaining long-term performance in AORFBs.

The secondary objective of the study [127] was to understand the relationship between structural modifications and physicochemical and electrochemical properties. These properties are crucial for optimizing AORFB performance as they directly influence the battery's energy density, stability, and efficiency. The study showed that functional groups such as secondary alcohol moieties improve the water solubility of viologen derivatives, achieving concentrations of up to 2.9 M for derivatives with ethanol groups (labeled as EtOH in Fig. 8) while increased molecular size and charge (such as ammonium groups) lead to higher solution viscosity, which can negatively affect the energy density by increasing the internal pressure and the energy cost of pumping in flow systems. Therefore, a tradeoff exists between solubility and viscosity. A similar trend was observed between the viscosity and

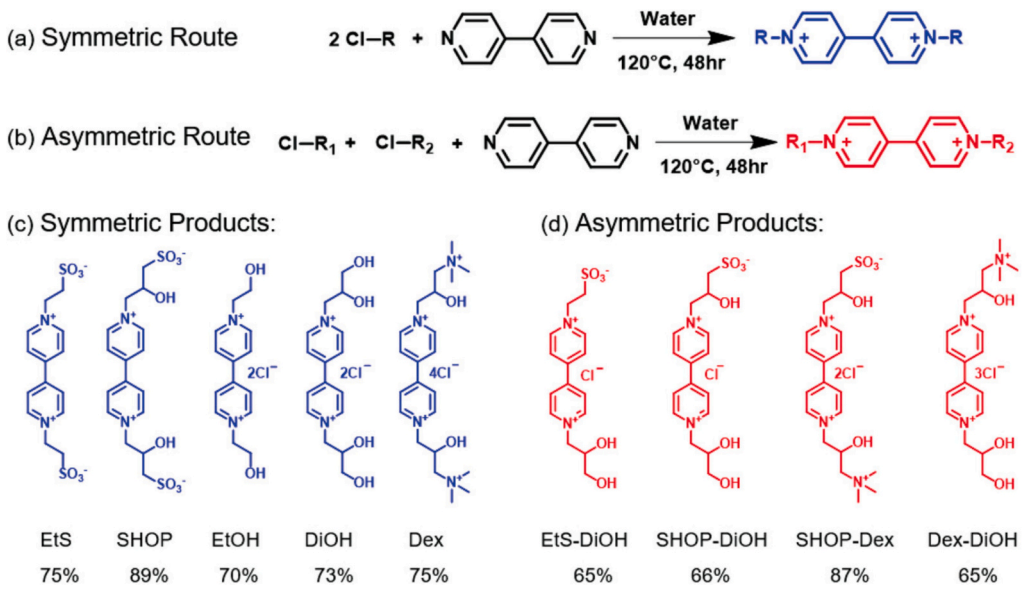

Fig. 8. Hydrothermal synthetic symmetric (*a*) and asymmetric (*b*) route. Structures of the symmetric (*c*) and asymmetric (*d*) viologens obtained. Reproduced from Ref. [127].

permeability relationship obtained from permeability studies on the Selemion DSVN anion exchange membrane. For example, EtOH and DiOH, which have hydroxyl functional groups, showed the highest permeability, 3.25×10^{-10} and 1.25×10^{-10} $cm^2\ s^{-1}$, respectively, but a lower viscosity, 2.5 and 3.0 mPa s at 1 M concentration, compared to Dex in which the positive charges on the quaternary ammonium resulted in the lowest permeability recorded (0.1×10^{-10} $cm^2\ s^{-1}$) with the disadvantage of the highest viscosity, 14.2 mPa s at 1 M concentration. In contrast, asymmetric Viologen, such as Dex-DiOH, due to the possibility of exploiting the advantages of different functional groups, displayed the best compromise between permeability (2.76×10^{-11} $cm^2\ s^{-1}$) and viscosity (3.75 mPa s at 1 M concentration), making it the best candidate for the battery test, despite its relatively lower solubility (2.7 M). A 2.5 M Dex-DiOH-Vi pure water solution was coupled with a 2.5 M methyl morpholine amide TEMPO (MMA-TEMPO) pure water solution for a battery test configuration, which showed an OCV of 1.09 V at 50 % SOC. After 250 cycles (14 days), the device showed a capacity utilization of 89.9 % and no apparent capacity decay, demonstrating high stability and low permeability as confirmed by post-mortem CV and NMR analysis.

Other authors explored the use of $[PyrTMAV]Cl_4$ (Fig. 9a) for AORFB applications by exploiting the same strategy of incorporating two-electron redox processes [108]. This viologen derivative is structurally modified by grafting it with pyrrolidinium and ammonium groups at the nitrogen atoms of the bipyridinium core. The asymmetric structure of $[PyrTMAV]Cl_4$ plays a critical role in its performance by mitigating intramolecular Coulomb repulsion, which can improve its electrochemical stability during cycling. The grafted groups also enhance solubility, with the compound exhibiting a high solubility of 1.71 M in deionized water and 1.68 M/1.61 M in 1.0 M/2.0 M NaCl solution, respectively, which is crucial for achieving higher energy storage capacities in flow battery applications. This viologen shows remarkable redox reversibility and stability, supporting a two-electron transfer process at −0.34 V and − 0.68 V *vs* SHE, enhancing energy density compared to traditional bipyridinium compounds, which typically rely on single-electron transfers. Furthermore, the compound demonstrates excellent resistance to crossover through the AMVN anion-exchange membrane. This is achieved due to the multi-charged nature of $[PyrTMAV]Cl_4$, effectively repelling the charged species from crossing the ion exchange membrane. This results in the maintenance of high battery efficiency over extended cycling periods, making it an attractive

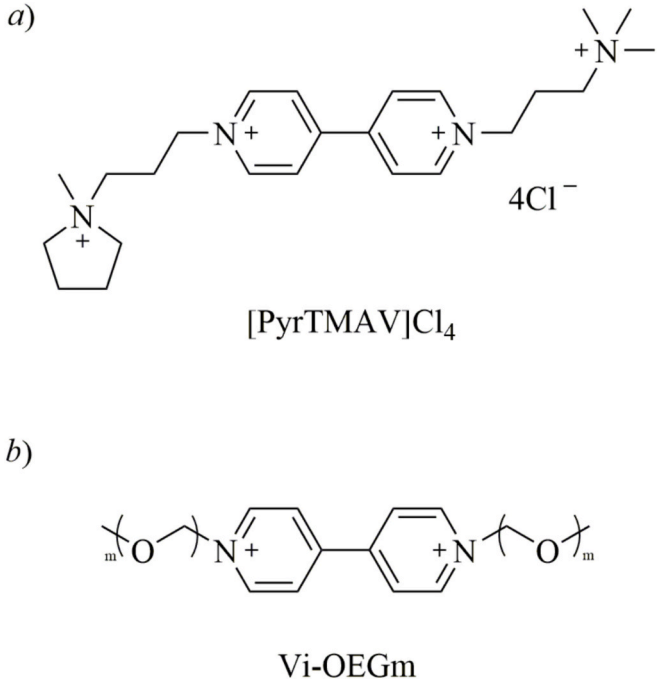

Fig. 9. Structures of Viologen derivatives.

candidate for large-scale energy storage applications. For the battery test, $[PyrTMAV]Cl_4$ was coupled with $[TMP\text{-}TEMPO]Cl_2$ described before. The battery operated with an open-circuit voltage of approximately 1.65 V, higher than the typical 1.45 V in other viologen systems. The AORFB with 0.1 M $[PyrTMAV]Cl_4$ anolyte and 0.2 M $[TMP\text{-}TEMPO]Cl_2$ catholyte showed a discharge capacity of 24.4 mAh, capacity retention of ~100 % after 238 cycles and energy efficiency of ~89 % and coulombic efficiency of ~100 %. Over 480 cycles, the battery exhibited a capacity degradation rate of 0.04 % per cycle and an energy efficiency of around 89 %, and, at SOC 100 %, this AORFB achieved a maximum power density of 184 mW cm^{-2} with a corresponding current density of 196 mA cm^{-2}. A high concentration AORFB was also tested at 20 mA cm^{-2} including 0.5 M $[PyrTMAV]Cl_4$ anolyte and 1.0 M [TMP-

TEMPO]Cl_2. It gave a capacity of ~133 mAh and a capacity degradation of 0.17 % per cycle over 176 cycles (mainly due to a higher degree of π-dimerization).

A common approach to improve viologen's electrochemical stability, cycling performance, and solubility is incorporating hydrophilic poly (ethylene glycol) (PEG) chains into their structure. This reduces the likelihood of dimerization of the radical cation (Vi•+), a significant cause of capacity fade in viologen-based systems, resulting in improved cycling stability. Additionally, the hydrophilic nature of the PEG side chains increases the solubility of the viologen in aqueous solutions, which is essential for achieving higher concentrations of active material in the electrolyte, thus improving the battery's energy density. Several PEGylated viologens have been synthesized, resulting in high molar mass molecules with the disadvantage of high viscosity solution leading to low energy and power density [128,129]. Yao et al. proposed an oligomeric ethylene glycol functionalization achievable in a one-step synthesis involving 4,4'-bipyridine and bromine functionalized oligo ethylene glycol (OEG), obtaining Vi-OEGm with m = 2,3 and 4 (Fig. 9b) [130].

The study focused on Vi-OEG2 and Vi-OEG3 since Vi-OEG4 resulted in a difficult-to-use compound. As expected, the introduction of OEG side chains slightly increased the viscosity of the solution to 1.21 and 1.20 mPa for 0.1 M Vi-OEG3 and Vi-OEG2, respectively, in a 0.1 M NaBr solution and reached a solubility in water of 1.6 M for m = 2 and 1.4 M for m = 3. In addition, the diffusion coefficient and the electron transfer rate constant were evaluated by Levich plot and Nicholson's method showing $D = 4.24 \times 10^{-6}$ cm^2 s^{-1}, $k^0 = 1.04 \times 10^{-2}$ cm s^{-1} for Vi-OEG2 and $D = 3.97 \times 10^{-6}$ cm^2 s^{-1}, $k^0 = 1.04 \times 10^{-2}$ cm s^{-1} for Vi-OEG3. The oligo(ethylene glycol)-substituted viologen derivatives exhibit superior electrochemical performance compared to their conventional counterparts. For instance, the tri(ethylene glycol)-substituted viologen (Vi-OEG3) exhibits high redox reversibility and stability in both its first (-0.55 V *vs.* SCE) and second one-electron redox process (-0.95 V *vs.* SCE), with CV curves remaining stable after 100 scan cycles. This two-electron storage capability significantly improves over conventional viologens, which struggle with insolubility issues in their neutral reduced form (MV^0). In symmetric cell tests involving only the first redox process, Vi-OEG3 outperforms other viologen derivatives, demonstrating better capacity retention over 19 days with a capacity decay rate of 0.047 % compared to 0.173 % per day for Vi-OEG2. The results suggest that the increased length of the OEG side chains directly correlates with improved cycling stability, as the bulky side chains effectively prevent the dimerization of the radical cation. The studies highlight the performance of Vi-OEG3 in a full-flow battery configuration, paired with N-(ferrocenylmethyl)-*N*, *N*-dimethyl-N-ethyl-ammonium bromide (FcNEBr) posolyte. The battery delivers a cell voltage of approximately 0.9 V and, with 0.5 M Vi-OEG3/FeNEBr solutions, maintains high-capacity retention even at high current densities. At 20 mA cm^{-2}, the battery achieves a capacity retention of 95 % and energy efficiency of 80.35 %. While the efficiency decreases at higher current densities, the coulombic efficiency remains above 99.6 %, indicating minimal side reactions and excellent charge recovery. The cycling performance of this flow cell was performed at 30 mA cm^{-2} in the range potential from 0.4 V to 1.15 V for 138 cycles, delivering a stable volumetric capacity of 12 Ah $L^{-1.}$ Additionally, the permeability of Vi-OEG3 through the anion exchange membrane is significantly lower than that of traditional viologens such as EV, which helps reduce crossover and improves the overall battery efficiency. Although these results are promising, battery tests involving two-electron redox processes resulted in an irreversible capacity loss in full cell cycling, probably due to the low redox potential of the second process favoring side reactions, so further work is needed to improve Vi^0 stability.

Achieving high energy density necessitates a high charge concentration. A common approach is increasing the electroactive species concentration; however, this may not represent the most efficient or straightforward strategy. For example, the design of a multi-electron transfer molecule can overcome this problem and open the way to a different approach, as the most commonly used electroactive species use one or two electron transfer processes. Huang et al. report a new π-conjugated heteroaromatic redox-active material hexaazatrinaphthalene tricarboxylic acid (HATNTA) (Fig. 10) as a promising anolyte for AORFB [131]. The synthesis of this molecule requires a one-step condensation of cyclohexane-1,2,3,4,5,6-hexone with *o*-phenylenediamine carboxylic acid derivative (Fig. 10), creating a π-conjugated heteroaromatic core and six nitrogen atoms that act as redox-active sites.

After showing a solubility of 0.583 M in a 1.5 M KOH aqueous solution and a viscosity of 21 and 30 mPa s for 0.05 M and 0.25 M HATNTA solution, respectively, the electrochemical properties of this molecule were tested by CV in a 1.5 M KOH solution. They revealed a diffusion-controlled reversible three-step, six-electron transfer reaction at different redox potentials (-0.69 V, -0.87 V, and -0.94 V *vs* Ag/AgCl). Moreover, LSV measurements *via* RDE showed a diffusion coefficient $D = 2.43 \times 10^{-6}$ cm^2 s^{-1} and an electron transfer rate constant $k^0 = 2.32 \times 10^{-3}$ cm s^{-1}. To confirm the performance of this molecule, a 0.05 M HATNTA-based cell was operated at a low current density (20 mA cm^{-2}); the discharge capacity was 7.3 Ah L^{-1}, corresponding to 91.2 % of the theoretical capacity of a 0.05 M molecule involved in a six-electron reversible redox process. This was also confirmed in the second battery test performed by coupling HATNTA with ferrocyanide, where two potential plateaus were observed from 0.5 V to 1.05 V and 1.05 V to 1.50 V, each contributing 1/3 and 2/3 of the total capacity respectively. The long-term cycling test was carried out by coupling a 0.05 M HATNTA in 1.5 M KOH solution with 0.05 M $K_4Fe(CN)_6$ in 1.3 M KOH solution, between 0.2 V and 1.6 V from 20 to 100 mA cm^{-2} showing a discharge capacity of 7.3 to 5.4 Ah L^{-1} (92.05 % to 66.92 % of the theoretical). At the same time, the coulombic efficiency remained constant at ~100 % at all current densities. Long-term galvanostatic-potentiostatic cycling was performed applying 40 mA cm^{-2} between 0.2 V and 1.6 V for 2000 cycles, showing a coulombic efficiency of ~100 %, an energy efficiency of ~79 % and a capacity fade of 0.0012 % per cycle demonstrating high stability. Finally, a high volumetric capacity flow battery was assembled with 0.25 M HATNTA and 0.25 M $K_4Fe(CN)_6$ in 0.5 M KOH. At 100 % SOC, the device exhibited a power density of 238 mW cm^{-2} and a high-capacity utilization from 94.19 % to 70.87 % at different current densities from 20 to 100 mA cm^{-2} and a columbic efficiency of ~100 %. After 80 cycles, the cell exhibited a specific capacity of 37.2 Ah L^{-1} with a capacity decay rate of 0.021 % per cycle.

Arylene diimides are a class of organic molecules based on large, planar, aromatic structures, most commonly used as pharmaceutical intermediates. Their cheap synthesis, with a 90 % yield of their electrolyte derivatives, makes them a good candidate for AORFB application. Although this class of materials has already been used in AORFB applications, they still suffer from low stability and poor water solubility. Liu et al. report three different quaternary ammonium arylene diimide derivatives that can be obtained in high yield [132]. Specifically, these three molecules differ in quaternary ammonium functionalization and π-system extension, as shown in Fig. 11.

Among them, NDI exhibited the highest solubility with a value of 1.0 M in a 2.0 M NaCl solution, followed by TPDI and PDI with a value of 0.14 M and 0.08 M, respectively, in the same conditions. The electrochemical properties were investigated by CV, NDI exhibits two one-electron redox processes at -0.09 V, $NDI^{2+} \leftrightarrow NDI^{+\cdot}$, and -0.46 V (*vs* NHE), $NDI^{+\cdot} \leftrightarrow NDI^0$; PDI presents two redox processes too, at -0.13 V, $PDI^{2+} \leftrightarrow PDI^{+\cdot}$, and -0.45 V, $PDI^{+\cdot} \leftrightarrow PDI^0$; while TPDI shows one redox process at -0.17 V, $TPDI^{6+} \leftrightarrow TPDI^{5+}$, and one at -0.35 V, $TPDI^{5+} \leftrightarrow TPDI^{4+}$. All peak currents of the redox processes showed a linear relationship with the square root of the scan rate, indicating reversible and diffusion-controlled behavior. The first redox process, studied by LSV analysis, showed a diffusion coefficient (D) of 6.18×10^{-6}, 1.03×10^{-6}, 9.07×10^{-6} cm^2 s^{-1}, for NDI, PDI and TPDI, respectively, while, for the second process, the D values were 1.10×10^{-5}, 8.67×10^{-6} and 1.06×10^{-4} cm^2 s^{-1}. The electron transfer rate

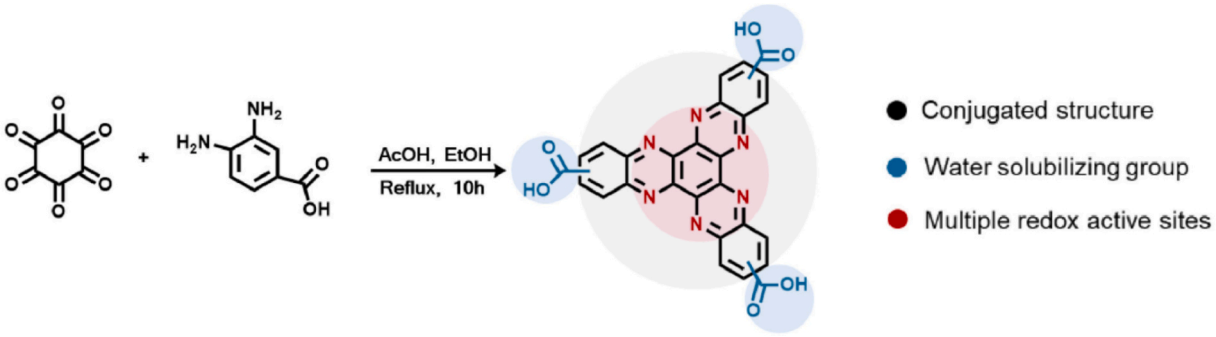

Fig. 10. Synthetic route for HATNTA. Reproduced from Ref. [131] with permission from Elsevier.

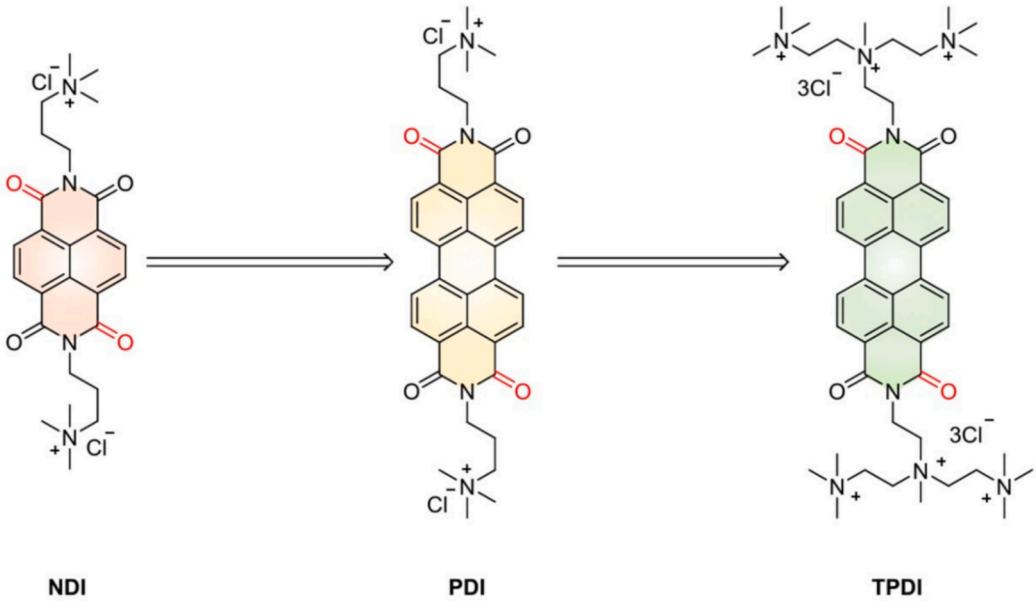

Fig. 11. Structure of arylene diimide derivatives: NDI, PDI, and TPDI. Adapted from Ref. [132] published in CCS Chemistry 2023.

constants were also evaluated and showed the following values: 5.73×10^{-3}, 3.93×10^{-4} and 2.42×10^{-3} cm $s^{-1}$for the first redox process and 2.07×10^{-2}, 1.05×10^{-3}, 7.29×10^{-3} cm s^{-1} for the second one. All three materials were used in a battery test to assess their performance in the field. A battery based on 0.1 M NDI/FcNCl in 2.0 M NaCl solution (ferrocene derivative) was assembled; at 100 % SOC the device had a peak power density of 98 mW cm^{-2} and, after 350 cycles at a current density of 40 mA cm^{-2}, a capacity of 4.36 Ah L^{-1} (81.34 % of the theoretical) and a capacity retention of 98.44 %, corresponding to a capacity decay of 0.0046 % per cycle. The battery was tested at different current densities, from 20 to 80 mA cm^{-2}, and showed almost 100 % coulombic efficiency; energy and voltage efficiency averaged 61 %. A higher concentration cell was assembled using a 0.5 M NDI solution; a decrease in cycle stability was observed, probably due to an increase in internal resistance, but the battery still showed a good capacity utilization of 22.08 Ah L^{-1} (82.39 % of the theoretical) and a peak power density of 100 mW cm^{-2} at 100 % SOC. The post-cycle test confirmed the cause of the capacity degradation, FcNCl crossover to the NDI side. The battery constructed with 0.02 M PDI/FcNCl revealed good cycle stability, maintaining a capacity retention, at 20 mA cm^{-2}, of 98.1 % over 1500 cycles, corresponding to a capacity decay of 0.0013 % per cycle with a maximum capacity of 0.96 Ah L^{-1} (89.72 % of theoretical). In addition, at lower concentrations, such as 0.01 M, no significant capacity degradation was observed over 10,000 cycles. The final tests were carried out with TPDI to see if the electrochemical properties of PDI could be transferred to a similar, more soluble compound. The 0.1 M TPDI/FcNCl battery showed a capacity utilization of 87.17 % and capacity retention of 97.22 % over 200 cycles at 20 mA cm^{-2}, corresponding to a capacity decay rate of 0.014 % per cycle and decreasing cell concentration up to 0.05 M led to a capacity retention rate of 95.50 % over 1600 cycles (decay of 0.0028 % per cycle), a maximum capacity of 2.33 Ah L^{-1} (86.98 % of theoretical), and a power density of 83 mW cm^{-2}. Finally, the authors attempted an electrolyte recovery experiment in which the post-cycle solution was purified *via* alumina column chromatography. However, compared to NDI and PDI, due to its high polarity, TPDI purification was unsuccessful.

Table 1 summarizes the key physicochemical properties of the catholytes discussed in the previous sections, including diffusion coefficients, solubility, redox potential, and kinetic rate constant in aqueous environments. These properties play a crucial role in determining the performance of catholytes in AORFBs, influencing factors such as energy density, power output, and long-term cyclability. This comparative overview highlights the strengths and limitations of each class of molecules, aiding in selecting suitable candidates for specific battery applications. In particular, the data in the table show how functional groups that can directly interact with the solvent, for example, *via* hydrogen bonding, tend to increase the solubility of the molecule and, combined with an asymmetry functionalization of the electrolyte, cooperate to increase its solubility, discouraging orientation toward a crystal structure that maximizes solute-solute interaction and

Table 1
Literature comparison of the physicochemical properties of organic electrolytes for application in aqueous organic redox flow batteries.

Electrolyte	Solubility[a] (M)	Redox potential (V *vs* SHE)	Diffusion coefficient ($cm^2\ s^{-1}$)	Kinetic rate constant ($cm\ s^{-1}$)	Reference
TEMPO	5.6 in 5.0 M LiTFSI	0.57	8.9×10^{-7}	[c]1.8×10^{-2}	[118]
TMP-TEMPO	2.16 in 2.0 M NaCl	0.98	4.12×10^{-6}	[d]1.65×10^{-2}	[108]
$Na_4[Fe^{II}(Dcbpy)_2(CN)_2]$	1.09	0.65[b]	2.3×10^{-6}	–	[120]
NGB/HP-β-CD	0.25 in 0.3 M HP-β-CD	0.70	2.80×10^{-7}	[c]1.52×10^{-3}	[121]
2,7-AQDS	1.39	-0.31 ($2e^-$)	1.6×10^{-6}	–	[88]
DHBQ	2.16 in 1.0 M KOH	-0.72 ($2e^-$)	–	–	[122]
Dex-DiOH-Vi	2.7	-0.34	3.49×10^{-6}	[e]1.21×10^{-1}	[127]
$[PyrTMAV]Cl_4$	1.71	-0.34 -0.68	3.85×10^{-6} 3.89×10^{-6}	[d]2.15×10^{-2} [d]2.05×10^{-2}	[108]
Vi-OEG3	1.4	-0.31 -0.71	3.97×10^{-6}	[d]1.04×10^{-2}	[130]
HATNTA	0.583 in 1.5 M KOH	-0.69[b] ($2e^-$) -0.87[b] ($2e^-$) -0.94[b] ($2e^-$)	2.43×10^{-6}	[d]2.32×10^{-3}	[131]
NDI	1.0 in 2.0 M NaCl	-0.10 -0.47	6.18×10^{-6} 1.10×10^{-5}	[d]5.73×10^{-3} [d]2.07×10^{-2}	[132]

[a] Maximum solubility in pure water (if not otherwise specified).
[b] V *vs* Ag/AgCl
[c] Calculated by Nicholson's method (CV/LSV)
[d] Calculated by Koutecký–Levich's method (LSV)
[e] Calculated by EIS

reducing solubility, and this is true for both small and large complex molecules; in addition, a supporting electrolyte can help to build up the required solubility. Although larger molecules offer greater tunability due to a broader range of functionalization possibilities and can achieve multi-electron redox processes at the desired redox potential, their constant aqueous solubility and kinetic rate remain challenging for AORFB application.

Table 2 provides an overview of the performance metrics of AORFBs utilizing the redox couples described in Table 1, paired with other redox couples. Comparing the performance of AORFBs reported by different research groups is inherently challenging due to the variability in experimental conditions, including differences in cell design, electrodes, membrane separators, electrolyte flow rates, and operational protocols. These factors can significantly influence AORFB performance, such as energy efficiency, power density, and cycling stability, making direct comparisons between studies complex and potentially misleading. To address this issue, we have limited our comparison to studies employing comparable AORFB configurations and operational parameters wherever possible. This approach minimizes variability and allows for a more meaningful assessment of the impact of the organic electrolytes on

Table 2
Comparison of electrochemical performance metrics for AORFBS employing organic electrolytes as catholytes or anolytes.

Catholyte	Anolyte	Theoretical OCV (V)	Theoretical capacity ($Ah\ L^{-1}$)	Capacity utilization	Capacity decay per cycle	Cycle	Other	Ref
TEMPO 0.5 M in 4.0 M LiTFSI	$(SPr)_2$ V 0.25 M in 4.0 M LiTFSI	1.08	13.4	69 %	0.048 %	285	CE = 99.5 %, EE = 82 %	[118]
TMP-TEMPO 1.0 M in 2.0 M NaCl	$[PyrTMAV]Cl_4$ 0.5 M in 2.0 M NaCl	1.58	26.8	90 %	0.17 %	176	EE ~ 87 %	[108]
$Na_4[Fe^{II}(Dcbpy)_2(CN)_2]$ 1.02 M in 0.1 M NaOH	SPr-Bpy 1.2 M in 1.2 M NaCl and 0.4 M CH_3CO_2Na	1.2	27.4	73 %	0.1 %	250	$E\text{-Den}_{max}$ = 17.5 $Wh\ L^{-1}$	[120]
NGB 0.1 M/HP-β-CD 0.2 M in 1.0 M NaCl	$(Spr)_2V$ 0.1 M in 1.0 M NaCl	1.22	2.68	21 %	0.008 %	250	CE ~ 99 %, P-Den_{max} = 36.7 $mW\ cm^{-2}$	[121]
HQS 0.2 M in 0.5 M Na_2SO_4	2,7-AQDS 0.2 M in 0.5 M Na_2SO_4	0.83	10.72	70 %	–	120	P-Den = 54.1 $mW\ cm^{-2}$, EE = 56 %, VE = 61 %	[88]
$K_4Fe(CN)_6$ 0.4 M in 1.0 M KOH	DHBQ 0.5 M in 1.0 M KOH	1.21	26.8	60 %	0.8 %	50	–	[122]
MMA-TEMPO 2.5 M	Dex-DiOH-Vi 2.5 M	1.09	67.0	89.9 %	~0 %	250	–	[127]
FeNEBr 0.5 M	Vi-OEG3 0.5 M in 2.0 M NaCl	0.95	13.4	95 %	0.0001 %	138	EE = 80.35 % CE = 99.6 %	[130]
$K_4Fe(CN)_6$ 0.25 M in 0.5 M KOH	HATNTA 0.25 M in 0.5 M KOH	1.24	40.2	94.2 %	0.021 %	80	CE ~ 100 %, P-Den = 238 $mW\ cm^{-2}$	[131]
FcNCl 0.5 M in 2.0 M NaCl	NDI 0.5 M in 2.0 M NaCl	1.07	26.8	82.4 %	0.073 %	100	P-Den_{max} = 100 $mW\ cm^{-2}$	[132]
FcNCl 0.02 M in 2.0 M NaCl	PDI 0.02 M in 2.0 M NaCl	1.06	1.07	89.72 %	0.0013 %	1500	CE ~ 100 %	[132]
FcNCl 0.1 M in 2.0 M NaCl	TPDI 0.1 M in 2.0 M NaCl	0.96	5.36	87.17 %	0.014 %	200	CE ~ 100 %	[132]

P-Den_{max} = Peak power density; E-Den_{max} = Peak energy density.

overall battery performance, providing more precise insights into their relative strengths and limitations.

Table 2 shows that theoretical capacities vary greatly depending on the electrolyte concentration, the number of redox processes, and the number of electrons involved. At present, small molecules such as TEMPO and viologen derivatives, which have good solubility, can achieve the highest capacity values in the table, and it is clear how a rational design aimed at limiting the crossover of electroactive species has managed to obtain low capacity decays per cycle. Although good theoretical capacity values were also obtained for molecules with an extended π system thanks to their multi-redox processes, their low solubility and low cycle stability led to a loss of capacity. Nevertheless, this demonstrates a sound proof of concept and allows new classes of molecules and strategies to be implemented in these devices.

4. Conclusions and outlook

This review examines recent advances in aqueous organic redox flow batteries (AORFBs), highlighting the potential of redox-active organic compounds as high-performance electrolyte materials. Organic materials that rely exclusively on earth-abundant elements can enhance sustainability and reduce supply chain vulnerability while enabling multi-electron transfer mechanisms without the challenges associated with multivalent inorganic ions. Despite this promise, AORFBs are still at an early stage of development compared to aqueous inorganic RFBs (such as all-vanadium or Zn/Br systems), and considerable work is required to overcome current limitations in voltage, capacity, and cycling stability before they become commercially viable.

Expanding the range of redox-active units and electrolyte materials in AORFBs is a priority. Many current organic electrolytes are based on a narrow set of structures. Still, future research should focus on developing highly stable, redox-reversible submolecular structures to support AORFBs with higher operating voltages and enhanced durability, especially for new catholytes. New classes of molecules have been studied through new organic synthesis methods and the help of computational chemistry without forgetting that multi-step synthesis and complex post-processing purification processes hinder the progress toward practical use. Moreover, given today's needs, green and safe organic molecules without environmental hazards are still indispensable for practical use. Additionally, creating oxygen-resistant materials would reduce costs and operational complexities by eliminating the need for oxygen isolation to prevent irreversible capacity loss.

Enhancing solubility in electrolyte solutions containing supporting salts is essential to improve the practical application of these materials. Many organic materials dissolve well in pure water, whereas their solubility is reduced when dissolved in inorganic salt solutions. Functionalizing the electroactive molecules with hydrophilic groups, such as hydroxyl and ammonium, overcomes this challenge by enhancing electrolyte-solvent interactions. This was demonstrated in literature studies on quinone derivatives, where the positioning of functional groups played a critical role in quinone electrochemistry. The selection of appropriate functional groups can also significantly enhance stability. For instance, viologen dimerization, a common side reaction responsible for capacity decay, can be mitigated by functionalization strategies that introduce electrostatic repulsion and steric hindrance, thereby improving electrolyte stability. Furthermore, incorporating different functional groups within the same molecule enables a more gradual modulation of electrolyte properties, as demonstrated by asymmetric viologens synthesized *via* hydrothermal methods, which exhibit intermediate properties not achievable with their symmetric counterpart. This approach has also been applied to metal complexes using organic ligands, where breaking the initial symmetry by introducing a second type of ligand allows for the modulation of the redox potential and increases the solubility of these complexes. Additionally, using organic molecules with an extended π-conjugated system has facilitated multi-electron redox processes, thereby increasing the energy density without increasing the concentration of the electroactive species. In addition, new doors may be opened to other strategies, such as ionic liquids (ILs), microemulsions, or, more generally, a self-assembly approach, which can increase solubility and stability in the presence of supporting electrolytes.

A significant barrier to AORFB efficiency is membrane crossover. Current ion-selective membranes must prevent redox species from crossing between anolyte and catholyte compartments while allowing ion transport to maintain charge balance. Advances in membrane technology, such as modifying pore sizes or adding ionic groups, could improve power density and cycling stability. A more precise understanding of the transport behavior of the redox species across membranes can guide the design of membranes and new electrolyte materials through rational functionalization. Different electrolyte characteristics can be tuned to maximize the membrane efficiency, such as molecular size, depending on the size of the membrane pores and ionic state, increasing hydrodynamic radius and repulsion with the same charged ionic groups on the membrane. On the other hand, symmetric AORFBs, which use molecules with multiple redox sites in both anolyte and catholyte roles, may eliminate crossover problems, thereby advancing the suitability of AORFBs for large-scale energy storage.

Research efforts conducted by the academic and industrial communities in AORFBs have led to significant advancements and remarkable performance improvements, particularly in increased energy density, power density, and cycling stability. However, challenges remain, especially in enhancing the long-term stability and scalability of organic electroactive materials. Understanding the reaction mechanisms within AORFBs is crucial for identifying optimal redox-active molecules, as this information can be rationalized and tuned through computational chemistry. Additionally, optimizing operational parameters such as flow rate, pH, viscosity, and temperature will enhance cell performance, reduce operational costs, and deepen our understanding of AORFB functioning. Indeed, continued investment in fundamental and applied research is essential to overcome existing barriers and accelerate the development of AORFB technologies, ensuring their future potential as a sustainable energy storage solution.

CRediT authorship contribution statement

Francesco Pileri: Writing – original draft, Investigation, Data curation. **Williane da Silva Freitas:** Writing – review & editing, Supervision, Methodology, Data curation, Conceptualization. **Alessandra D'Epifanio:** Writing – review & editing, Resources, Project administration, Funding acquisition, Conceptualization. **Barbara Mecheri:** Writing – review & editing, Supervision, Resources, Project administration, Methodology, Funding acquisition, Data curation, Conceptualization.

Declaration of competing interest

The authors declare that they have no known competing financial interests or personal relationships that could have appeared to influence the work reported in this paper.

Acknowledgments

Authors acknowledge financial support from “ORgANics for Green Electrochemical Energy Storage Project (ORANGEES)” funded by MASE (The Italian Ministry of Environment and Energy Security) “PT 2019-2021, DD 27.10.2021 bando a, DD 05.08.2022”. This work has also received funding from the European Union – Next Generation EU in response to the MUR (The Italian Ministry of University and Research) call “PRIN (Project of National Interest) 2022”: Project code: 202233PT4N.

Data availability

Data will be made available on request.

References

[1] C. Zhang, Z. Yuan, X. Li, Designing better flow batteries: an overview on fifty Years' research, ACS Energy Lett. 9 (2024) 3456–3473, https://doi.org/10.1021/acsenergylett.4c00773.

[2] C.G. Cannon, P.A.A. Klusener, N.P. Brandon, A.R.J. Kucernak, Aqueous redox flow batteries: small organic molecules for the positive electrolyte species, ChemSusChem 16 (2023), https://doi.org/10.1002/cssc.202300303.

[3] R. Chen, Redox flow batteries: electrolyte chemistries unlock the thermodynamic limits, Chem. Asian J. 18 (2022), https://doi.org/10.1002/asia.202201024.

[4] M. Mansha, A. Ayub, I.A. Khan, S. Ali, A.S. Alzahrani, M. Khan, M. Arshad, A. Rauf, S. Akram Khan, Recent development of electrolytes for aqueous organic redox flow batteries (Aorfbs): current status, challenges, and prospects, Chem. Rec. 24 (2024) e202300284, https://doi.org/10.1002/tcr.202300284.

[5] B. Péceli, I. Szatmári, G. Paternò, A. Rossi, A. D'Epifanio, S. Licoccia, B. Mecheri, Innovative Redox Flow Battery Systems for the Implementation of Flexible Microgrids, in: 2018 IEEE International Conference on Environment and Electrical Engineering and 2018 IEEE Industrial and Commercial Power Systems Europe (EEEIC / I&CPS Europe), 2018: pp. 1–6. doi:https://doi.org/10.1109/EEEIC.2018.8494574.

[6] M. Skyllas-Kazacos, C. Menictas, Vanadium redox flow batteries, in: L.F. Cabeza (Ed.), Encyclopedia of Energy Storage, Elsevier, Oxford, 2022, pp. 407–422, https://doi.org/10.1016/B978-0-12-819723-3.00050-0.

[7] C. Busacca, O. Di Blasi, G. Giacoppo, N. Briguglio, V. Antonucci, A. Di Blasi, High performance electrospun nickel manganite on carbon nanofibers electrode for vanadium redox flow battery, Electrochim. Acta 355 (2020), https://doi.org/10.1016/j.electacta.2020.136755.

[8] C. Menictas, M. Skyllas-Kazacos, Next-Generation Vanadium Flow Batteries, Flow Batteries, in, 2023, pp. 673–687, https://doi.org/10.1002/9783527832767.ch30.

[9] M. Branchi, M. Gigli, B. Mecheri, D. De Porcellinis, S. Licoccia, A. D'Epifanio, Poly(phenylene sulfide sulfone) based membranes with improved stability for vanadium redox flow batteries, J. Mater. Chem. A Mater. 5 (2017) 18845–18853, https://doi.org/10.1039/c7ta03046k.

[10] M. Branchi, M. Gigli, B. Mecheri, F. Zurlo, S. Licoccia, A. D'Epifanio, Highly ion selective hydrocarbon-based membranes containing sulfonated hypercrosslinked polystyrene nanoparticles for vanadium redox flow batteries, J. Membr. Sci. 563 (2018) 552–560, https://doi.org/10.1016/j.memsci.2018.06.022.

[11] M. Gigli, B. Mecheri, S. Licoccia, A. D'Epifanio, Crosslinked sulfonated poly (phenylene sulfide sulfone) membranes for vanadium redox flow batteries, SM&T 28 (2021), https://doi.org/10.1016/j.susmat.2021.e00249.

[12] A. Parasuraman, T.M. Lim, C. Menictas, M. Skyllas-Kazacos, Review of material research and development for vanadium redox flow battery applications, Electrochim. Acta 101 (2013) 27–40, https://doi.org/10.1016/j.electacta.2012.09.067.

[13] J. Winsberg, T. Hagemann, T. Janoschka, M.D. Hager, U.S. Schubert, Redox-flow batteries: from metals to organic redox-active materials, Angew. Chem. 129 (2017) 702–729, https://doi.org/10.1002/ange.201604925.

[14] Y. Cho, H. Kye, B.G. Kim, J.E. Kwon, Redox active viologen derivatives for aqueous and non-aqueous organic redox flow batteries applications, J. Ind. Eng. Chem. 136 (2024) 73–88, https://doi.org/10.1016/j.jiec.2024.02.037.

[15] P. Fischer, P. Mazúr, J. Krakowiak, Family tree for aqueous organic redox couples for redox flow battery electrolytes: a conceptual review, Molecules 27 (2022), https://doi.org/10.3390/molecules27020560.

[16] M. Shoaib, P. Vallayil, N. Jaiswal, P. Iyapazham Vaigunda Suba, S. Sankararaman, K. Ramanujam, V. Thangadurai, Advances in redox flow batteries – A Comprehensive Review on Inorganic and Organic Electrolytes and Engineering Perspectives, Adv. Energy Mater. 14 (2024), https://doi.org/10.1002/aenm.202400721.

[17] F. Zhu, Q. Chen, Y. Fu, Perspectives on aqueous organic redox flow batteries, Green Energy Environ. (2024), https://doi.org/10.1016/j.gee.2024.08.003.

[18] S. Giri, I. Dash, Ferrocene to functionalized ferrocene: a versatile redox-active electrolyte for high-performance aqueous and non-aqueous organic redox flow batteries, J. Mater. Chem. A Mater. 11 (2023) 16458–16493, https://doi.org/10.1039/D3TA01747H.

[19] B. Huskinson, M.P. Marshak, C. Suh, S. Er, M.R. Gerhardt, C.J. Galvin, X. Chen, A. Aspuru-Guzik, R.G. Gordon, M.J. Aziz, A metal-free organic-inorganic aqueous flow battery, Nature 505 (2014) 195–198, https://doi.org/10.1038/nature12909.

[20] J. Luo, B. Hu, C. Debruler, T.L. Liu, A π-conjugation extended Viologen as a two-Electron storage Anolyte for Total organic aqueous redox flow batteries, Angew. Chem. 57 (2018) 231–235, https://doi.org/10.1002/anie.201710517.

[21] T. Janoschka, N. Martin, U. Martin, C. Friebe, S. Morgenstern, H. Hiller, M. D. Hager, U.S. Schubert, An aqueous, polymer-based redox-flow battery using non-corrosive, safe, and low-cost materials, Nature 527 (2015) 78–81, https://doi.org/10.1038/nature15746.

[22] K. Lin, Q. Chen, M.R. Gerhardt, L. Tong, S.B. Kim, L. Eisenach, A.W. Valle, D. Hardee, R.G. Gordon, M.J. Aziz, M.P. Marshak, Alkaline quinone flow battery, Science 349 (2015) (1979) 1529–1532, https://doi.org/10.1126/science.aab3033.

[23] M. Al Raihan, C.A. Dyker, Status and prospects for symmetric organic redox flow batteries, J. Energy Chem. 100 (2025) 125–143, https://doi.org/10.1016/j.jechem.2024.08.016.

[24] B. Liu, Y. Li, G. Jia, T. Zhao, Recent advances in redox flow batteries employing metal coordination complexes as redox-active species, Electrochem. Energy Rev. 7 (2024), https://doi.org/10.1007/s41918-023-00205-6.

[25] K. Peng, G. Tang, C. Zhang, X. Yang, P. Zuo, Z. Xiang, Z. Yao, Z. Yang, T. Xu, Progress and prospects of pH-neutral aqueous organic redox flow batteries: electrolytes and membranes, J. Energy Chem. 96 (2024) 89–109, https://doi.org/10.1016/j.jechem.2024.04.031.

[26] B. Lu, K. Yu, W. Shao, Y. Ji, F. Zhang, Organic redox-active molecules for alkaline aqueous redox flow batteries, Curr. Opin. Green Sustain. Chem. 47 (2024), https://doi.org/10.1016/j.cogsc.2024.100905.

[27] D. Emmel, S. Kunz, N. Blume, Y. Kwon, T. Turek, C. Minke, D. Schröder, Benchmarking organic active materials for aqueous redox flow batteries in terms of lifetime and cost, Nat. Commun. 14 (2023), https://doi.org/10.1038/s41467-023-42450-9.

[28] D. Cremoncini, G. Di Lorenzo, G.F. Frate, A. Bischi, A. Baccioli, L. Ferrari, Techno-economic analysis of aqueous organic redox flow batteries: stochastic investigation of capital cost and levelized cost of storage, Appl. Energy 360 (2024), https://doi.org/10.1016/j.apenergy.2024.122738.

[29] L. Tang, P. Leung, M.R. Mohamed, Q. Xu, S. Dai, X. Zhu, C. Flox, A.A. Shah, Q. Liao, Capital cost evaluation of conventional and emerging redox flow batteries for grid storage applications, Electrochim. Acta 437 (2023), https://doi.org/10.1016/j.electacta.2022.141460.

[30] J. Luo, B. Hu, M. Hu, Y. Zhao, T.L. Liu, Status and prospects of organic redox flow batteries toward sustainable energy storage, ACS Energy Lett.. 4 (2019) 2220–2240, https://doi.org/10.1021/acsenergylett.9b01332.

[31] K. Gong, Q. Fang, S. Gu, S.F.Y. Li, Y. Yan, Nonaqueous redox-flow batteries: organic solvents, supporting electrolytes, and redox pairs, Energy Environ. Sci. 8 (2015) 3515–3530, https://doi.org/10.1039/c5ee02341f.

[32] C.S. Sevov, R.E.M. Brooner, E. Chénard, R.S. Assary, J.S. Moore, J. Rodríguez-López, M.S. Sanford, Evolutionary Design of low Molecular Weight Organic Anolyte Materials for applications in nonaqueous redox flow batteries, J. Am. Chem. Soc. 137 (2015) 14465–14472, https://doi.org/10.1021/jacs.5b09572.

[33] Q. Chen, M.R. Gerhardt, M.J. Aziz, Dissection of the voltage losses of an acidic Quinone redox flow battery, J. Electrochem. Soc. 164 (2017) A1126–A1132, https://doi.org/10.1149/2.0721706jes.

[34] D. Chen, Z. Yuan, W. Duan, Y. He, T. Li, C. Kang, Q. Dai, X. Li, Porous membrane with high selectivity for alkaline quinone-based flow batteries, ACS Appl. Mater. Interfaces 12 (2020) 48533–48541, https://doi.org/10.1021/acsami.0c13172.

[35] M.T. Tsehaye, G. Mourouga, T.J. Schmidt, J.O. Schumacher, S. Velizarov, B. Van der Bruggen, F. Alloin, C. Iojoiu, Towards optimized membranes for aqueous organic redox flow batteries: correlation between membrane properties and cell performance, Renew. Sust. Energ. Rev. 173 (2023), https://doi.org/10.1016/j.rser.2022.113059.

[36] R. Yang, S. Zhang, Y. Zhu, A high performance, stable anion exchange membrane for alkaline redox flow batteries, J. Power Sources 594 (2024), https://doi.org/10.1016/j.jpowsour.2023.233974.

[37] S. Sreenath, P.S. Nayanthara, C.M. Pawar, M.C. Noufal, R.K. Nagarale, Phenolic triamine dangling poly(VDF-co-HFP) anion exchange membrane for all aqueous organic redox flow battery, J. Energy Stor. 40 (2021), https://doi.org/10.1016/j.est.2021.102689.

[38] Y. Xia, M. Ouyang, V. Yufit, R. Tan, A. Regoutz, A. Wang, W. Mao, B. Chakrabarti, A. Kavei, Q. Song, A.R. Kucernak, N.P. Brandon, A cost-effective alkaline polysulfide-air redox flow battery enabled by a dual-membrane cell architecture, Nat. Commun. 13 (2022), https://doi.org/10.1038/s41467-022-30044-w.

[39] G. Shukla, G. Kumbhar, C. Bruggeman, S.J. Curley, C.R. Szczepanski, D.P. Hickey, R.C. Ferrier, Poly(vinylidene difluoride-co-hexafluoropropylene) grafted with polyether amphoteric ion-exchange membranes for aqueous redox flow batteries, ACS Appl. Energy Mater. (2024), https://doi.org/10.1021/acsaem.4c00014.

[40] S. Shi, A.Z. Weber, A. Kusoglu, Structure/property relationship of Nafion XL composite membranes, J. Membr. Sci. 516 (2016) 123–134, https://doi.org/10.1016/j.memsci.2016.06.004.

[41] J. Ye, L. Xia, H. Li, F.P.G. de Arquer, H. Wang, The critical analysis of membranes toward sustainable and efficient vanadium redox flow batteries, Adv. Mater. 36 (2024), https://doi.org/10.1002/adma.202402090.

[42] N. Zhao, A. Platt, H. Riley, R. Qiao, R. Neagu, Z. Shi, Strategy towards high ion selectivity membranes for all-vanadium redox flow batteries, J. Energy Stor. 72 (2023), https://doi.org/10.1016/j.est.2023.108321.

[43] B.G. Thiam, S. Vaudreuil, Recent membranes for vanadium redox flow batteries, J. Electrochem. Soc. 168 (2021) 070553, https://doi.org/10.1149/1945-7111/ac163c.

[44] J. Montero, W. da Silva Freitas, B. Mecheri, M. Forchetta, P. Galloni, S. Licoccia, A. D'Epifanio, A neutral-pH aqueous redox flow battery based on sustainable organic electrolytes, ChemElectroChem 10 (2023), https://doi.org/10.1002/celc.202201002.

[45] K. Amini, A.N. Shocron, M.E. Suss, M.J. Aziz, Pathways to high-power-density redox flow batteries, ACS Energy Lett. 8 (2023) 3526–3535, https://doi.org/10.1021/acsenergylett.3c01043.

[46] D.G. Kwabi, K. Lin, Y. Ji, E.F. Kerr, M.A. Goulet, D. De Porcellinis, D.P. Tabor, D. A. Pollack, A. Aspuru-Guzik, R.G. Gordon, M.J. Aziz, Erratum: alkaline Quinone flow battery with Long lifetime at pH 12, Joule 2 (2018) 1907–1908, https://doi.org/10.1016/j.joule.2018.08.013.

[47] T. Janoschka, N. Martin, M.D. Hager, U.S. Schubert, An aqueous redox-flow battery with high capacity and power: the TEMPTMA/MV system, Angew. Chem. Int. Ed. 55 (2016) 14427–14430, https://doi.org/10.1002/anie.201606472.
[48] M. Hu, W. Wu, J. Luo, T.L. Liu, Desymmetrization of Viologen Anolytes empowering energy dense, ultra stable flow batteries toward Long-duration energy storage, Adv. Energy Mater. 12 (2022), https://doi.org/10.1002/aenm.202202085.
[49] X.-L. Lv, P.T. Sullivan, W. Li, H.-C. Fu, R. Jacobs, C.-J. Chen, D. Morgan, S. Jin, D. Feng, Modular dimerization of organic radicals for stable and dense flow battery catholyte, Nat. Energy 8 (2023) 1109–1118, https://doi.org/10.1038/s41560-023-01320-w.
[50] B. Zhang, Z. Yang, Q. Liu, Y. Liu, S. Jiang, X. Zhang, E. Zhang, K. Wang, S. Zhang, High-performance aqueous organic redox flow battery enabled by sulfonated anthrone-containing poly(aryl ether ketone) membranes, J. Membr. Sci. 706 (2024), https://doi.org/10.1016/j.memsci.2024.122968.
[51] S. Dumkrang, K. Li, L. Intakhuen, K. Punyawudho, S. Koonaphapdeelert, Development of aqueous organic flow battery using SPEEK membrane and eco-friendly electrolytes, Curr. J. Appl. 24 (2024), https://doi.org/10.55003/cast.2024.258288.
[52] D. De Porcellinis, B. Mecheri, A. D'Epifanio, S. Licoccia, S. Granados-Focil, M. J. Aziz, Sulfonated poly (ether ether ketone) as cation exchange membrane for alkaline redox flow batteries, J. Electrochem. Soc. 165 (2018) A1137–A1139, https://doi.org/10.1149/2.1291805jes.
[53] E. Hampson, J.C. Duburg, J. Casella, T.J. Schmidt, L. Gubler, A simple approach to balancing conductivity and capacity fade in vanadium redox flow batteries by the tunable pretreatment of polybenzimidazole membranes, Chem. Eng. J. 485 (2024), https://doi.org/10.1016/j.cej.2024.149930.
[54] Y.H. Wan, J. Sun, Q.P. Jian, X.Z. Fan, T.S. Zhao, A Nafion/polybenzimidazole composite membrane with consecutive proton-conducting pathways for aqueous redox flow batteries, J. Mater. Chem. A Mater. 10 (2022) 13021–13030, https://doi.org/10.1039/D2TA01746F.
[55] H. Yu, Y. Wu, W. Xu, Y. Zheng, J. Ding, Y. Wang, Z. Xu, Pd2+-coordinated polybenzimidazole membranes with fast and selective ion transport for alkaline aqueous organic redox flow battery, J. Membr. Sci. 713 (2025), https://doi.org/10.1016/j.memsci.2024.123320.
[56] S. Kunz, T.T. Bui, D. Emmel, J. Janek, D. Henkensmeier, D. Schröder, Aqueous redox flow cells utilizing Verdazyl cations enabled by Polybenzimidazole membranes, ChemSusChem (2024), https://doi.org/10.1002/cssc.202400550.
[57] T. Hagemann, M. Strumpf, E. Schröter, C. Stolze, M. Grube, I. Nischang, M. D. Hager, U.S. Schubert, (2,2,6,6-Tetramethylpiperidin-1-yl)oxyl-containing Zwitterionic polymer as Catholyte species for high-capacity aqueous polymer redox flow batteries, Chem. Mater. 31 (2019) 7987–7999, https://doi.org/10.1021/acs.chemmater.9b02201.
[58] Y. Liu, G.H. Wen, J. Liang, S.S. Bao, J. Wei, H. Wang, P. Zhang, M. Zhu, Q. Jia, J. Ma, L.M. Zheng, Z. Jin, Aqueous colloid flow batteries based on redox-reversible Polyoxometalate clusters and size-exclusive membranes, ACS Energy Lett. 8 (2023) 387–397, https://doi.org/10.1021/acsenergylett.2c02121.
[59] J. Montero, P. Navalpotro, A. Depifanio, B. Mecheri, S. Licoccia, J. Carretero-González, Redox-active coordination polymers as bifunctional electrolytes in slurry-based aqueous batteries at neutral pH, J. Electroanal. Chem. 895 (2021), https://doi.org/10.1016/j.jelechem.2021.115442.
[60] W. Cheng, C. Liu, T. Tong, R. Epsztein, M. Sun, R. Verduzco, J. Ma, M. Elimelech, Selective removal of divalent cations by polyelectrolyte multilayer nanofiltration membrane: role of polyelectrolyte charge, ion size, and ionic strength, J. Membr. Sci. 559 (2018) 98–106, https://doi.org/10.1016/j.memsci.2018.04.052.
[61] C.A. MacHado, G.O. Brown, R. Yang, T.E. Hopkins, J.G. Pribyl, T.H. Epps, Redox flow battery membranes: improving battery performance by leveraging structure-property relationships, ACS Energy Lett. 6 (2021) 158–176, https://doi.org/10.1021/acsenergylett.0c02205.
[62] Y. Sato, A. Narita, Y. Kaneko, A. Negishi, K. Nozaki, T. Kato, Characterization of carbon materials for redox flow battery electrodes by voltage-step Coulometry, ECS Trans. 75 (2017) 37–47, https://doi.org/10.1149/07518.0037ecst.
[63] X. Wei, W. Pan, W. Duan, A. Hollas, Z. Yang, B. Li, Z. Nie, J. Liu, D. Reed, W. Wang, V. Sprenkle, Materials and Systems for Organic Redox Flow Batteries: status and challenges, ACS Energy Lett. 2 (2017) 2187–2204, https://doi.org/10.1021/acsenergylett.7b00650.
[64] H. Zhang, T. Ding, R. Zhao, R. Kuang, K. Lu, S. Lu, A bifunctional electrocatalytic graphite felt for stable aqueous zinc-polyiodide flow batteries, J. Power Sources 612 (2024), https://doi.org/10.1016/j.jpowsour.2024.234798.
[65] J. Tao, Z. Chen, L. Qi, M. Zheng, One-Dimensional Analytical Model for Optimizing Porosity Distribution of Multi-Layered Electrode in Redox Flow Cells, Applied Energy Symposium 2020: Low Carbon Cities and Urban Energy Systems, 2020.
[66] X. Zhang, X. Liu, H. Zhang, Z. Wang, Y. Zhang, G. Li, M.J. Li, G. He, Robust Chalcogenophene Viologens as Anolytes for Long-life aqueous organic redox flow batteries with high battery voltage, ACS Appl. Mater. Interfaces 14 (2022) 48727–48733, https://doi.org/10.1021/acsami.2c14195.
[67] M. Meskinfam Langroudi, C.S. Pomelli, R. Giglioli, C. Chiappe, M. Aysla Costa de Oliveira, B. Mecheri, S. Licoccia, A. D'Epifanio, Interaction of vanadium species with a functionalized graphite electrode: a combined theoretical and experimental study for flow battery applications, J. Power Sources 420 (2019) 134–142, https://doi.org/10.1016/j.jpowsour.2019.02.083.
[68] I. Cheng, Batteries: recent advances in carbon materials, C (Basel) 3 (2017) 1, https://doi.org/10.3390/c3010001.
[69] Z. Manzoor Bhat, M. Furquan, M. Aurang Zeb Gul Sial, U. Alam, A. Saeed Alzahrani, M. Qamar, Implications of electrode modifications in aqueous organic redox flow batteries, J. Energy Chem. 95 (2024) 499–510, https://doi.org/10.1016/j.jechem.2024.03.058.
[70] M.A.C. de Oliveira, M. Brunet Cabré, C. Schröder, H. Nolan, F. Pota, J.A. Behan, F. Barrière, K. McKelvey, P.E. Colavita, Single-entity electrochemistry of N-doped graphene oxide nanostructures for improved kinetics of Vanadyl oxidation, Small (2024), https://doi.org/10.1002/smll.202405220.
[71] R. Chen, P. Zhang, Z. Chang, J. Yan, T. Kraus, Grafting and Solubilization of redox-active organic materials for aqueous redox flow batteries, ChemSusChem 16 (2023) e202201993, https://doi.org/10.1002/cssc.202201993.
[72] X. Zhang, H. Gao, W. Jin, Y. Huang, J. Xu, J. Cao, Oxygen-vacancy-enriched MgO/carbon composite as a highly efficient electrocatalyst for phenazine/dihydrophenazine redox reaction of aqueous phenazine redox flow battery, Mater. Today Energy 43 (2024), https://doi.org/10.1016/j.mtener.2024.101587.
[73] P.S. Borchers, M. Strumpf, C. Friebe, I. Nischang, M.D. Hager, J. Elbert, U. S. Schubert, Aqueous redox flow battery suitable for high temperature applications based on a tailor-made ferrocene copolymer, Adv. Energy Mater. 10 (2020), https://doi.org/10.1002/aenm.202001825.
[74] F. Ai, Z. Wang, N.-C. Lai, Q. Zou, Z. Liang, Y.-C. Lu, Heteropoly acid negolytes for high-power-density aqueous redox flow batteries at low temperatures, Nat. Energy 7 (2022) 417–426, https://doi.org/10.1038/s41560-022-01011-y.
[75] Z. Huang, P. Zhang, X. Gao, D. Henkensmeier, S. Passerini, R. Chen, Unlocking simultaneously the temperature and electrochemical windows of aqueous Phthalocyanine electrolytes, ACS Appl. Energy Mater. 2 (2019) 3773–3779, https://doi.org/10.1021/acsaem.9b00467.
[76] M. Chen, R. Chen, I. Zhitomirsky, G. He, K. Shi, Redox-active molecules for aqueous electrolytes of energy storage devices: a review on fundamental aspects, current progress, and prospects, Mater. Sci. Eng. R. Rep. 161 (2024), https://doi.org/10.1016/j.mser.2024.100865.
[77] Y.Y. Lai, X. Li, K. Liu, W.Y. Tung, C.F. Cheng, Y. Zhu, Stable low-cost organic dye Anolyte for aqueous organic redox flow battery, ACS Appl. Energy Mater. 3 (2020) 2290–2295, https://doi.org/10.1021/acsaem.9b01735.
[78] W. Zhang, Y. Chen, T.-R. Wu, X. Xia, J. Xu, Z. Chen, J. Cao, D.-Y. Wu, Computational design of phenazine derivative molecules as redox-active electrolyte materials in alkaline aqueous organic flow batteries, New J. Chem. 46 (2022) 11662–11668, https://doi.org/10.1039/D2NJ01769E.
[79] R. Chen, Toward high-voltage, Energy-Dense, and Durable Aqueous Organic Redox Flow Batteries: Role of the Supporting Electrolytes, ChemElectroChem 6 (2019) 603–612, https://doi.org/10.1002/celc.201801505.
[80] R.P. Fornari, M. Mesta, J. Hjelm, T. Vegge, P. De Silva, Molecular engineering strategies for symmetric aqueous organic redox flow batteries, ACS Mater. Lett. 2 (2020) 239–246, https://doi.org/10.1021/acsmaterialslett.0c00028.
[81] L. Tong, M.A. Goulet, D.P. Tabor, E.F. Kerr, D. De Porcellinis, E.M. Fell, A. Aspuru-Guzik, R.G. Gordon, M.J. Aziz, Molecular engineering of an alkaline naphthoquinone flow battery, ACS Energy Lett. 4 (2019) 1880–1887, https://doi.org/10.1021/acsenergylett.9b01321.
[82] K. Peng, Y. Li, G. Tang, Y. Liu, Z. Yang, T. Xu, Solvation regulation to mitigate the decomposition of 2,6-dihydroxyanthraquinone in aqueous organic redox flow batteries, energy, Environ. Sci. 16 (2023) 430–437, https://doi.org/10.1039/D2EE03617G.
[83] C. Ye, A. Wang, C. Breakwell, R. Tan, C. Grazia Bezzu, E. Hunter-Sellars, D. R. Williams, N.P. Brandon, P.A.A. Klusener, A.R. Kucernak, K.E. Jelfs, N. B. McKeown, Q. Song, Development of efficient aqueous organic redox flow batteries using ion-sieving sulfonated polymer membranes, Nat. Commun. 13 (2022), https://doi.org/10.1038/s41467-022-30943-y.
[84] L. Guglielmero, M.M. Langroudi, M. Al Khatib, M.A.C. de Oliveira, B. Mecheri, M. De Leo, A. Mezzetta, L. Guazzelli, R. Giglioli, A.D. Epifanio, R. Pogni, C. Chiappe, C.S. Pomelli, Electrochemical and spectroscopic study of vanadyl acetylacetonate–ionic liquids interactions, Electrochim. Acta 373 (2021), https://doi.org/10.1016/j.electacta.2021.137865.
[85] W. Lee, K. In Shim, G. Park, J.W. Han, Y. Kwon, Rational design of composite supporting electrolyte required for achieving high performance aqueous organic redox flow battery, J. Chem. Eng. 464 (2023), https://doi.org/10.1016/j.cej.2023.142661.
[86] X. Yuan, M. Huang, Z. Liang, Effect of variable viscosity of electrolytes on mass transport and electrochemical reactions in aqueous organic redox flow battery, Int. J. Heat Mass Transf. 205 (2023), https://doi.org/10.1016/j.ijheatmasstransfer.2023.123924.
[87] W. Dean, M. Muñoz, J. Noh, Y. Liang, W. Wang, B. Gurkan, Tuning and high throughput experimental screening of eutectic electrolytes with co-solvents for redox flow batteries, Electrochim. Acta 474 (2024) 143517, https://doi.org/10.1016/j.electacta.2023.143517.
[88] G. Yang, Y. Zhu, Z. Hao, Q. Zhang, Y. Lu, Z. Yan, J. Chen, An aqueous all-Quinone-based redox flow battery employing neutral electrolyte, Adv. Energy Mater. 14 (2024), https://doi.org/10.1002/aenm.202400022.
[89] S. Huang, H. Zhang, M. Salla, J. Zhuang, Y. Zhi, X. Wang, Q. Wang, Molecular engineering of dihydroxyanthraquinone-based electrolytes for high-capacity aqueous organic redox flow batteries, Nat. Commun. 13 (2022), https://doi.org/10.1038/s41467-022-32424-8.
[90] P. Mazúr, J. Charvát, J. Mrlík, J. Pocedič, J. Akrman, L. Kubáč, B. Řeháková, J. Kosek, Evaluation of electrochemical stability of sulfonated anthraquinone-based acidic electrolyte for redox flow battery application, Molecules 26 (2021), https://doi.org/10.3390/molecules26092484.
[91] M. Wu, M. Bahari, Y. Jing, K. Amini, E. Fell, T. George, R. Gordon, M. Aziz, Highly stable low redox potential Quinone for aqueous flow batteries, Batter Supercaps (2021), https://doi.org/10.26434/chemrxiv-2021-rjzdn.

[92] D.G. Kwabi, A.A. Wong, M.J. Aziz, Rational evaluation and cycle life improvement of Quinone-based aqueous flow batteries guided by in-line optical spectrophotometry, J. Electrochem. Soc. 165 (2018) A1770–A1776, https://doi.org/10.1149/2.0791809jes.
[93] J.E. dos S. Clarindo, R.N.P. Colombo, G.C. Sedenho, L.C.I. Faria, T. Bertaglia, F.C. D.A. Lima, R. da Silva Gomes, M.J. Aziz, F.N. Crespilho, Molecular mechanism and electrostatic effect enabling symmetric all-Quinone aqueous redox flow batteries, ACS Sustain. Chem. Eng. 12 (2024) 11488–11497, https://doi.org/10.1021/acssuschemeng.3c08218.
[94] D.P. Tabor, R. Gómez-Bombarelli, L. Tong, R.G. Gordon, M.J. Aziz, A. Aspuru-Guzik, Mapping the frontiers of quinone stability in aqueous media: implications for organic aqueous redox flow batteries, J. Mater. Chem. A Mater. 7 (2019) 12833–12841, https://doi.org/10.1039/c9ta03219c.
[95] C.O. Wilhelmsen, S.B. Kristensen, O. Nolte, I.A. Volodin, J.V. Christiansen, T. Isbrandt, T. Sørensen, C. Petersen, T.E. Sondergaard, K. Lehmann Nielsen, T. O. Larsen, J.C. Frisvad, M.D. Hager, U.S. Schubert, J. Muff, J.L. Sørensen, Demonstrating the use of a fungal synthesized Quinone in a redox flow battery, Batter Supercaps 6 (2023), https://doi.org/10.1002/batt.202200365.
[96] G. Park, W. Lee, Y. Kwon, Aqueous organic redox flow batteries using naphthoquinone and iodide maintaining pH of electrolytes desirably by adoption of carboxylic acid functionalized carbon nanotube catalyst, Int. J. Energy Res. 46 (2022) 3362–3375, https://doi.org/10.1002/er.7386.
[97] L. Xu, Q. Wang, D. Guo, J. Xu, J. Cao, A quaternized anthraquinone derivative for pH-neutral aqueous organic redox flow batteries, New J. Chem. 47 (2023) 11216–11221, https://doi.org/10.1039/D3NJ00784G.
[98] M. Huang, W. Li, D. Lin, K. Wan, Z. Fu, Z. Xiang, Z. Liang, Thermodynamic regulation of electrolyte to achieve air-tolerant viologen-based flow battery, Energy Stor. Mater. 67 (2024), https://doi.org/10.1016/j.ensm.2024.103267.
[99] W. Wu, J. Luo, F. Wang, B. Yuan, T.L. Liu, A self-trapping, bipolar viologen bromide electrolyte for redox flow batteries, ACS Energy Lett. 6 (2021) 2891–2897, https://doi.org/10.1021/acsenergylett.1c01146.
[100] A. Korshunov, A. Gibalova, M. Grünebaum, B.J. Ravoo, M. Winter, I. Cekic-Laskovic, Host-guest interactions enhance the performance of Viologen electrolytes for aqueous organic redox flow batteries, Batter Supercaps 4 (2021) 923–928, https://doi.org/10.1002/batt.202100018.
[101] A. Korshunov, A. Gibalova, M. Gruenebaum, B.J. Ravoo, M. Winter, I. Cekic-Laskovic, Supramolecular Viologen-Cyclodextrin electrolytes for aqueous organic redox flow batteries, ACS Appl. Energy Mater. 4 (2021) 12353–12364, https://doi.org/10.1021/acsaem.1c02156.
[102] W. Jin, Y. Chen, L.-K. Chen, D.-Y. Wu, J. Xu, J. Cao, Computational design of C-substituted paraquat/diquat derivatives for neutral aqueous organic redox flow batteries, New J. Chem. 48 (2024) 10884–10890, https://doi.org/10.1039/D4NJ01001A.
[103] S. Jin, E.M. Fell, L. Vina-Lopez, Y. Jing, P.W. Michalak, R.G. Gordon, M.J. Aziz, Near neutral pH redox flow battery with low permeability and Long-lifetime Phosphonated Viologen active species, Adv. Energy Mater. 10 (2020), https://doi.org/10.1002/aenm.202000100.
[104] R. Rubio-Presa, L. Lubián, M. Borlaf, E. Ventosa, R. Sanz, Addressing practical use of Viologen-derivatives in redox flow batteries through molecular engineering, ACS Mater. Lett. 5 (2023) 798–802, https://doi.org/10.1021/acsmaterialslett.2c01105.
[105] M. Pan, L. Gao, J. Liang, P. Zhang, S. Lu, Y. Lu, J. Ma, Z. Jin, Reversible redox chemistry in Pyrrolidinium-based TEMPO radical and extended Viologen for high-voltage and Long-life aqueous redox flow batteries, Adv. Energy Mater. 12 (2022), https://doi.org/10.1002/aenm.202103478.
[106] Y. Liu, Y. Li, P. Zuo, Q. Chen, G. Tang, P. Sun, Z. Yang, T. Xu, Screening Viologen derivatives for neutral aqueous organic redox flow batteries, ChemSusChem 13 (2020) 2245–2249, https://doi.org/10.1002/cssc.202000381.
[107] O. Nolte, P. Rohland, N. Ueberschaar, M.D. Hager, U.S. Schubert, Stability of TMA-TEMPO-based aqueous electrolytes for redox-flow batteries, J. Power Sources 525 (2022), https://doi.org/10.1016/j.jpowsour.2022.230996.
[108] M. Pan, Z. Jin, T. Zhao, J. Sun, Z. You, E. Pahuyo Delmo, M. Farhadpour, Z. Wu, M. Shao, Highly soluble and crossover-free all-organic redox pair using N-heterocycle-linked TEMPO and two-electron-capable bipyridinium towards high performance aqueous flow batteries, J. Chem. Eng. 496 (2024). doi:https://doi.org/10.1016/j.cej.2024.153504.
[109] M. Artault, G. Gonzalez, P. Damlin, J. Toivola, A. Mailman, J. Hannonen, P. M. Pihko, P. Peljo, Azoniafluorenones: a new family of two-Electron storage electrolytes for sustainable near-neutral pH aqueous organic flow battery, Adv. Energy Mater. (2024), https://doi.org/10.1002/aenm.202401635.
[110] A. Hamza, F.B. Németh, Á. Madarász, A. Nechaev, P. Pihko, P. Peljo, I. Pápai, N-alkylated pyridoxal derivatives as negative electrolyte materials for aqueous organic flow batteries: computational screening, Chem. Eur. J. (2023), https://doi.org/10.26434/chemrxiv-2023-bzc6w.
[111] S. Kunz, M. Janse Van Rensburg, D.S. Pietruschka, A.J. Achazi, D. Emmel, F. Kerner, D. Mollenhauer, H.A. Wegner, D. Schröder, Unraveling the electrochemistry of Verdazyl species in acidic electrolytes for the application in redox flow batteries, Chem. Mater. 34 (2022) 10424–10434, https://doi.org/10.1021/acs.chemmater.2c02279.
[112] M. Qin, G. Wu, K. Zheng, X. Yu, J. Xu, J. Cao, A highly water-soluble phenoxazine quaternary ammonium compound catholyte for pH-neutral aqueous organic redox flow batteries, J. Energy Stor. 102 (2024), https://doi.org/10.1016/j.est.2024.114162.
[113] Z. Zhao, T. Li, C. Zhang, M. Zhang, S. Li, X. Li, Air-stable naphthalene derivative-based electrolytes for sustainable aqueous flow batteries, Nat. Sustain. 7 (2024) 1273–1282, https://doi.org/10.1038/s41893-024-01415-6.
[114] X. Liu, H. Zhang, C. Liu, Z. Wang, X. Zhang, H. Yu, Y. Zhao, M.-J. Li, Y. Li, Y.-L. He, G. He, Commercializable naphthalene Diimide Anolytes for neutral aqueous organic redox flow batteries, Angew. Chem. Int. Ed. 63 (2024) e202405427, https://doi.org/10.1002/anie.202405427.
[115] B. Liu, W. Wei, Y. Wang, M. Song, Y. Chen, H. Chen, L. Chen, Q. Dai, S. Yao, J. Xu, G. Jia, T. Zhao, Design and synthesis of low-potential and cycling-stable cobalt dicarboxylate bipyridine complexes for high-voltage aqueous organic redox flow batteries, Sci. Bull. (Beijing) 69 (2024) 1632–1636, https://doi.org/10.1016/j.scib.2024.03.019.
[116] S. Pang, L. Li, Y. Ji, P. Wang, A multielectron and high-potential Spirobifluorene-based Posolyte for aqueous redox flow batteries, Angew. Chem. Int. Ed. 63 (2024) e202410226, https://doi.org/10.1002/anie.202410226.
[117] C. Wang, Y. Wang, M. Tao, B. Yu, K. Zhang, J. Wei, Y. Liu, P. Zhang, G. Ding, Z. Tie, J. Cao, Z. Jin, Highly water-soluble 6-Quinoxalinecarboxylic acid for high-voltage aqueous organic redox flow batteries, ACS Appl. Energy Mater. 5 (2022) 10379–10384, https://doi.org/10.1021/acsaem.2c01978.
[118] E. Pedraza, C. de la Cruz, A. Mavrandonakis, E. Ventosa, R. Rubio-Presa, R. Sanz, S.T. Senthilkumar, P. Navalpotro, R. Marcilla, Unprecedented aqueous solubility of TEMPO and its application as high capacity Catholyte for aqueous organic redox flow batteries, Adv. Energy Mater. 13 (2023), https://doi.org/10.1002/aenm.202301929.
[119] W. Zhou, W. Liu, M. Qin, Z. Chen, J. Xu, J. Cao, J. Li, Fundamental properties of TEMPO-based catholytes for aqueous redox flow batteries: effects of substituent groups and electrolytes on electrochemical properties, solubilities and battery performance, RSC Adv. 10 (2020) 21839–21844, https://doi.org/10.1039/D0RA03424J.
[120] X. Li, P. Gao, Y.Y. Lai, J.D. Bazak, A. Hollas, H.Y. Lin, V. Murugesan, S. Zhang, C. F. Cheng, W.Y. Tung, Y.T. Lai, R. Feng, J. Wang, C.L. Wang, W. Wang, Y. Zhu, Symmetry-breaking design of an organic iron complex catholyte for a long cyclability aqueous organic redox flow battery, Nat. Energy 6 (2021) 873–881, https://doi.org/10.1038/s41560-021-00879-6.
[121] K. Yang, T. Zhang, Q. Li, Z. Peng, J. Ning, R. Sun, S. Jiang, B. Li, Assembling-induced redox property adjustment of Fe(III)/Fe(IV) electroredox couple-based commercial dye catholyte via bio-inspired multicoordination sphere construction strategy for stable aqueous redox flow batteries, Energy Stor. Mater. 71 (2024), https://doi.org/10.1016/j.ensm.2024.103648.
[122] J.Y. Kim, J.W. Ho, D. Kim, M.W. Moon, G.H. Choi, P.J. Yoo, Unveiling dominant impact of electrochemical stability on performance deterioration in alkaline redox flow batteries utilizing different benzoquinone derivatives, J. Power Sources 611 (2024), https://doi.org/10.1016/j.jpowsour.2024.234766.
[123] X. Liu, C. Bao, Z. Wang, C. Liu, X. Zhang, S. Yang, Y.K. Li, G.L. Hou, N. Yan, G. He, Meta-substituted thienoviologen with enhanced radical stability via π-π interaction modulation for neutral aqueous organic flow batteries, Energy Stor. Mater. 73 (2024), https://doi.org/10.1016/j.ensm.2024.103824.
[124] S. Hwang, M. Oh, K.J. Lee, C.S. Jin, S.K. Park, C. Seo, S.H. Yeon, D.H. Kim, D. Gueon, Y.K. Han, K.H. Shin, Integration of functional groups to enhance the solubility and stability of Viologen in aqueous organic redox flow batteries, ACS Appl. Mater. Interfaces 16 (2024) 28645–28654, https://doi.org/10.1021/acsami.4c04528.
[125] L. Wang, K. Wan, X. Yuan, Z. Xiang, Z. Fu, Z. Liang, Steric hindrance shielding viologen against alkali attack in realizing ultrastable aqueous flow batteries, J. Energy Chem. 97 (2024) 529–534, https://doi.org/10.1016/j.jechem.2024.06.016.
[126] D.Y. Nikumbe, R.G. Pandi, A. Saha, B. Bhatt, S. Bhai, B. Ganguly, S.S. Kumar, R. K. Nagarale, Mono-methyl viologen: a promising anolyte for alkaline aqueous redox flow batteries, J. Mater. Chem. A Mater. 12 (2024) 25934–25947, https://doi.org/10.1039/D4TA03959A.
[127] P.T. Sullivan, H. Liu, X.L. Lv, S. Jin, W. Li, D. Feng, Viologen Hydrothermal Synthesis and Structure–Property Relationships for Redox Flow Battery Optimization, Adv. Energy Mater. 13 (2023). doi:https://doi.org/10.1002/aenm.202203919.
[128] M. Serhan, M. Sprowls, D. Jackemeyer, M. Long, I.D. Perez, W. Maret, N. Tao, E. Forzani, Synthesis and Characterization of TEMPO- and Viologen-Polymers for Water-Based Redox-Flow Batteries, Polym Chem 2019-November, 2019, https://doi.org/10.1039/C5PY01602A.
[129] K. Peng, P. Sun, Z. Yang, T. Xu, A PEGylated Viologen for crossover-free and high-capacity pH-neutral aqueous organic redox flow batteries, Batter Supercaps 6 (2023), https://doi.org/10.1002/batt.202200426.
[130] Y. Yao, W. Ma, J. Lei, Z. Wang, Y.C. Lu, L. Liu, Nonionic oligo(ethylene glycol)-substituted viologen negolytes for aqueous organic redox flow batteries, J. Mater. Chem. A Mater. 11 (2023) 12984–12991, https://doi.org/10.1039/d2ta09177a.
[131] B. Hu, H. Li, H. Fan, J. Song, A long-lifetime aqueous organic redox flow battery utilizing multi-redox anolyte, Energy Stor. Mater. 59 (2023), https://doi.org/10.1016/j.ensm.2023.102789.
[132] X. Liu, X. Zhang, C. Bao, Z. Wang, H. Zhang, G. Li, N. Yan, M.J. Li, G. He, Arylene Diimide derivatives as Anolyte materials with two-Electron storage for Ultrastable neutral aqueous organic redox flow batteries, CCS Chem. 5 (2023) 2334–2347, https://doi.org/10.31635/ccschem.022.202202336.